CANCER

Promoting antibody-dependent cellular phagocytosis for effective macrophage-based cancer immunotherapy

Xu Cao[1]†, Jing Chen[1]†, Bolei Li[1]†, Jessica Dang[1], Wencan Zhang[2], Xiancai Zhong[2], Chongkai Wang[3], Mustafa Raoof[4], Zuoming Sun[2], Jianhua Yu[1,5,6], Marwan G. Fakih[3], Mingye Feng[1]*

Macrophages are essential in eliciting antibody-dependent cellular phagocytosis (ADCP) of cancer cells. However, a satisfactory anticancer efficacy of ADCP is contingent on early antibody administration, and resistance develops along with cancer progression. Here, we investigate the mechanisms underlying ADCP and demonstrate an effective combinatorial strategy to potentiate its efficacy. We identified paclitaxel as a universal adjuvant that efficiently potentiated ADCP by a variety of anticancer antibodies in multiple cancers. Rather than eliciting cytotoxicity on cancer cells, paclitaxel polarized macrophages toward a state with enhanced phagocytic ability. Paclitaxel-treated macrophages down-regulated cell surface CSF1R whose expression was negatively correlated with patient survival in multiple malignancies. The suppression of CSF1R in macrophages enhanced ADCP of cancer cells, suggesting a role of CSF1R in regulating macrophage phagocytic ability. Together, these findings define a potent strategy for using conventional anticancer drugs to stimulate macrophage phagocytosis and promote the therapeutic efficacy of clinical anticancer antibodies.

INTRODUCTION

Advances in cancer genetics have led to the discovery of specific cancer-addicted genes and sprung cancer therapy from conventional chemotherapeutics into molecular-targeted medicine. Central among these is the development of cancer-specific antibodies and their wide application in a broad spectrum of malignancies. The introduction of rituximab, an anti-CD20 monoclonal antibody approved by the U.S. Food and Drug Administration (FDA) for non-Hodgkin's lymphoma (NHL) in 1997 (*1*), marked the beginning of the "targeted therapy era" of human cancer. The inclusion of rituximab into the established CHOP (cyclophosphamide, vincristine, doxorubicin, and prednisone) regimen has reduced the overall NHL mortality and improved the long-term prognosis of NHL patients (*2*). In addition to rituximab, targeting human HER2 receptor with trastuzumab has also revolutionized the treatment for a subtype of breast cancer expressing HER2 protein (*3*). Likewise, cetuximab has been widely used for the treatment of human epidermal growth factor receptor (EGFR)–positive colorectal cancer (*4*) and squamous cell carcinoma of the head and neck (SCCHN) (*5*).

Anticancer antibodies function by binding to the surface antigens on cancer cells, which may lead to two layers of effects. First, antibodies achieve tumor killing by acting as agonists or antagonists for cellular signaling. Antibodies can block the intrinsic growth/survival signaling or promote cell death signaling in cancer cells, exemplified by trastuzumab-mediated suppression of HER2 receptor signaling and cetuximab-mediated inhibition of EGFR signaling (*6*, *7*). In addition, antibodies can be used to target the tumor-infiltrating immune cells or stromal cells and vascular cells in the tumor microenvironment (TME) by blocking immunosuppressive signals or checkpoints to evoke an anticancer immune response or inhibiting angiogenesis and the tumor-favorable microenvironment, exemplified by T cell immune checkpoint inhibitors ipilimumab and pembrolizumab for blocking cytotoxic lymphocyte antigen-4 (CTLA4) and programmed cell death protein 1 (PD1) and bevacizumab for blocking VEGFR (vascular endothelial growth factor receptor) (*8*–*12*). Second, in addition to antigen recognition, the Fc region of an antibody interacts with the complement system to induce complement-dependent cytotoxicity, or with the Fc receptors on natural killer (NK) cells or macrophages to induce antibody-dependent cellular cytotoxicity (ADCC) or antibody-dependent cellular phagocytosis (ADCP) (*13*). Despite this, it remains unclear to what extent does the underlying immune activity account for the clinical efficacy of the individual anticancer antibody. Nevertheless, activating the immune components is an attractive approach to augment the anticancer activities of these antibodies while sparing normal tissues due to the restricted expression of antigens on tumor tissues.

Among the immune cellularity in TME, tumor-associated macrophages (TAMs) are the most abundant immune cells in nearly all types of malignancies (*14*–*16*). The induction of macrophage-mediated ADCP has demonstrated clinical efficacy and appears to be a major mechanism for the anticancer effects of many therapeutic antibodies. The binding of the Fc region of antibodies to Fcγ receptors (FcγRs) on macrophages triggers ADCP through the phosphorylation of the immunoreceptor tyrosine-based activation motif (ITAM) of FcγRs, which activates downstream signaling through Rac–GEFs (guanine nucleotide exchange factors) to induce phagocytosis. FcγRIIB is the only FcγR with an immunoreceptor tyrosine-based inhibition motif (ITIM), whose phosphorylation transduces a negative signaling cascade to inhibit phagocytosis (*17*, *18*). Trastuzumab and rituximab have been shown to rely on the activation of FcγRs for efficient tumor killing in breast cancer and lymphoma preclinical models, while their anticancer efficacy was enhanced in mice deficient in FcγRIIB (*19*). ADCP was also shown to be a driving

[1]Department of Immuno-Oncology, Beckman Research Institute, City of Hope, Duarte, CA 91010, USA. [2]Department of Immunology and Theranostics, Arthur Riggs Diabetes and Metabolism Research Institute, Beckman Research Institute, City of Hope, Duarte, CA 91010, USA. [3]Department of Medical Oncology and Therapeutics Research, City of Hope, Duarte, CA 91010, USA. [4]Department of Surgery, City of Hope, Duarte, CA 91010, USA. [5]Department of Hematology and Hematopoietic Cell Transplantation, City of Hope, Duarte, CA 91010, USA. [6]Hematologic Malignancies and Stem Cell Transplantation Institute, City of Hope, Duarte, CA 91010, USA.
*Corresponding author. Email: mfeng@coh.org
†These authors contributed equally to this work.

mechanism for the anticancer activity of daratumumab, an anti-CD38 therapeutic antibody, in lymphoma and multiple myeloma (*20*). In addition, ADCP contributed to the cytotoxicity of human monoclonal antibodies targeting CD20 in chronic lymphocytic leukemia (*21*). Thus, harnessing macrophage-mediated ADCP demonstrates considerable promise as an emerging novel and effective immunotherapeutic strategy for the battle against cancer.

The clinical observation of a positive correlation between rituximab efficacy and TAM abundance in NHL patient biopsies suggests a critical role of TAMs in mediating the efficacy of monoclonal antibodies (*22*). However, the efficacy is normally limited at the site of bulky diseases, which represent a late stage of tumor progression (*23*, *24*), indicating a likely phagocytic defect of TAMs along with tumorigenesis. In addition, therapeutic antibodies need to reach a local threshold to effectively induce ADCP, which often cannot be achieved through most of the current antibody administration routes (*13*, *25*–*28*). Therefore, for therapeutic antibodies to achieve the desired efficacy, the combinatorial agents may be required to restore (or enhance) macrophage phagocytic ability or lower the threshold for ADCP activation. A high dose of the alkylating drug cyclophosphamide combined with alemtuzumab, an anti-CD52 monoclonal antibody for human lymphoma, has recently been found to achieve the clearance of lymphoma cells by promoting phagocytosis via TAMs (*29*). In addition, the stimulation of TAMs with CpG oligodeoxynucleotide, a Toll-like receptor (TLR9) agonist, rewired the metabolic programs of macrophages to counteract anti-phagocytic signals and enabled phagocytosis of pancreatic ductal adenocarcinoma cells (*30*). These findings suggest that agents promoting the phagocytic ability of macrophages may overcome the barriers limiting tumor cell phagocytosis by TAMs and serve as a rational combination for monoclonal therapeutic antibodies.

In the present work, we demonstrated essential roles of macrophage phagocytosis in mediating the anticancer activity of monoclonal antibodies including rituximab, trastuzumab, and cetuximab. Through a novel long-term phagocytosis-based high-throughput screening (HTS) platform, we identified and validated paclitaxel as a therapeutic agent to universally enhance the efficacy of monoclonal anticancer antibodies in vitro and in vivo, mainly by stimulating macrophage phagocytosis instead of eliciting cell toxicity. Mechanistically, paclitaxel promoted FcγR-dependent phagocytosis signaling pathways in macrophages. In addition, paclitaxel remodeled the expression of surface membrane proteins on macrophages, including a down-regulation of CSF1R. Our data suggested that the suppression of cell surface CSF1R on macrophages enhanced ADCP toward cancer cells, indicating an unprecedented role of CSF1R in regulating macrophage phagocytosis.

RESULTS

Macrophage-based HTS identifies paclitaxel as a universal ADCP-potentiating agent for multiple therapeutic antibodies

While the involvement of therapeutic antibodies in inducing ADCP for cancer cell elimination has been investigated in individual cancer models in previous studies (*20*, *21*, *31*–*35*), whether ADCP functions as a generally applicable mechanism for multiple cancers has not been well established. In most tumors, TAMs are derived from circulating monocytes that originated from bone marrow progenitor cells (*15*, *16*, *36*). Therefore, we used a bone marrow–derived macrophage (BMDM) model to evaluate the efficacy of ADCP in multiple cancer cell models.

We showed that treating EGFR-expressing SCCHN cell line SCC9 and colorectal cancer cell lines SW480 and DLD1 with various concentrations of cetuximab inhibited the growth of SCC9 cells in a dose-dependent manner but had no such inhibitory effects on the growth of SW480 and DLD1 cells (fig. S1A), which bear functional KRAS mutations ($Gly^{12}Val$ in SW480 and $Gly^{13}Asp$ in DLD1), consistent with the notion that KRAS mutations confer resistance to EGFR signaling blockade (*37*). In addition, cetuximab treatment demonstrated minimal effect on inducing apoptosis (fig. S1B). We then tested the effects of trastuzumab or rituximab on HER2-expressing breast cancer line SKBR3 or CD20-expressing NHL cell line Raji, respectively. Trastuzumab partially inhibited the growth of SKBR3 cells, while rituximab exhibited no inhibition on the growth of Raji cells (fig. S1C). These data suggested that the direct cytotoxicity toward cancer cells in inhibiting their growth or viability was not consistent for therapeutic antibodies. In contrast, in the presence of BMDMs, cetuximab demonstrated strong anticancer effects regardless of the KRAS mutation status of the cells (fig. S1A). We showed that cetuximab induces strong phagocytosis of cancer cells by macrophages (fig. S1D). The expression of EGFR was also found to correlate with clinical response to cetuximab (fig. S1E). Similarly, the anticancer effectiveness of trastuzumab or rituximab was markedly enhanced upon the inclusion of macrophages (fig. S1C) through the induction of phagocytosis of cancer cells (fig. S1, F and G). To further establish the role of macrophages, we derived human primary macrophages from peripheral blood monocytes and performed phagocytosis assays with various antibodies and human cancer cell lines. All the abovementioned therapeutic antibodies were able to significantly induce phagocytosis of corresponding human cancer cells by human macrophages (Fig. 1A).

Next, we tested the anticancer efficacy of ADCP in mice engrafted with SW480 cells. We showed that cetuximab largely inhibited tumor development when administered at the same day when SW480 cells were transplanted to the mice intraperitoneally (Fig. 1B and fig. S2A), despite SW480 cells being highly resistant to cetuximab-induced apoptosis or inhibition of cell proliferation (fig. S1, A and B). The therapeutic effect was nearly abolished in mice when their peritoneal macrophages were depleted via administration of clodronate liposome (fig. S2, A to D), indicating a key role of macrophages in the anticancer effects of cetuximab in vivo.

Our results suggested that modulation of macrophage phagocytosis could be a promising strategy to enhance the anticancer efficacy of therapeutic antibodies and to overcome cancer cells' resistance to treatment. Therefore, we reasoned that the strategies to promote macrophage-mediated ADCP may overcome the barriers limiting the efficacy of therapeutic antibodies for cancer treatment. To address this, we set up a long-term phagocytosis assay to evaluate the efficacy of ADCP by quantifying cancer cells that survive ADCP when cocultured with BMDMs (Fig. 1C). A panel of 147 FDA-approved anticancer small molecules that have demonstrated clinical safety were screened in the long-term phagocytosis assay, with DLD1 as the target cells in the presence of cetuximab (table S1 and Fig. 1, C to E). We observed that the vast majority of the chemotherapies demonstrated subtle effects on cancer cell phagocytosis (around line $y = 1$); in contrast, kinase inhibitors showed a strong tendency to suppress the effect of cetuximab (below line $y = 1$) in inducing ADCP. We identified paclitaxel, imiquimod, and cabazitaxel as

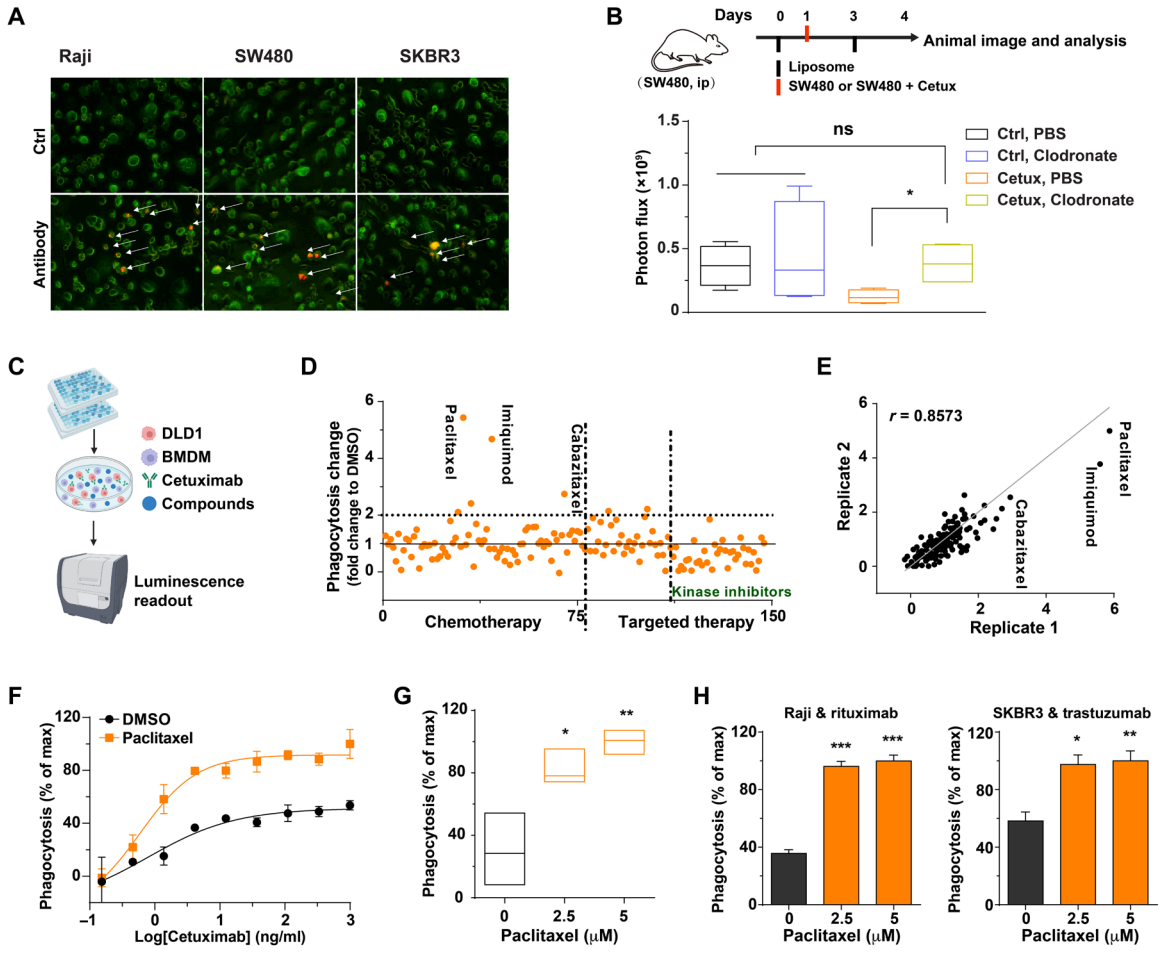

Fig. 1. Macrophage-based HTS identifies paclitaxel as a universal ADCP-potentiating agent for multiple therapeutic antibodies. (**A**) Evaluation of anticancer antibody–induced phagocytosis of various human cancer cells with human peripheral blood monocyte–derived macrophages by microscopy. Representative figures of three independent experiments. (**B**) Growth of tumors developed by SW480 cells in RAG2$^{-/-}$γc$^{-/-}$ mice. Mice were intraperitoneally (ip) injected with SW480 cells and treated with vehicle (Ctrl) or cetuximab. The mice were treated with control liposomes or clodronate liposomes, and tumor growth was measured by bioluminescence. $n = 4$; *$P < 0.05$ [one-way analysis of variance (ANOVA)]. ns, not significant. (**C**) Experimental schematic showing the design of the high-throughput screen. (**D**) Phagocytosis-based high-throughput screens of 147 FDA-approved anticancer small-molecule compounds. DLD1 cells were subjected to luminescence-based phagocytosis assay in the presence of cetuximab. Spots represent individual compounds. Phagocytosis was normalized to dimethyl sulfoxide (DMSO) control. $Y = 1$ indicated phagocytosis induced by compounds equaled to that by DMSO control. (**E**) Correlation of the change of phagocytosis rates between the two replicates. Spots represent individual compounds. (**F**) Paclitaxel (2.5 μM) enhanced the potency of cetuximab-mediated phagocytosis of DLD1 cells, measured by a luminescence-based phagocytosis assay. Experiments were performed in duplicate for each concentration. (**G**) Cetuximab-mediated phagocytosis of SW480 cells was enhanced by various concentrations of paclitaxel, measured by a luminescence-based phagocytosis assay. $n = 3$; *$P < 0.05$ and **$P < 0.01$ (one-way ANOVA). (**H**) Paclitaxel enhanced rituximab-mediated phagocytosis of Raji cells and trastuzumab-mediated phagocytosis of SKBR3 cells by human peripheral blood monocyte–derived macrophages, measured by a luminescence-based phagocytosis assay. $n = 3$; *$P < 0.05$, **$P < 0.01$, and ***$P < 0.001$ (one-way ANOVA).

agents significantly potentiating cetuximab-induced ADCP by macrophages (Fig. 1D). The effects of these three top hits were further examined in a dose-dependent manner. We showed that, among this three, paclitaxel is most potent in promoting ADCP (fig. S3A); thus, we decided to further pursue the efficacy and therapeutic potential of using paclitaxel as an adjuvant to antibody-mediated cancer immunotherapy using ADCP. We showed that paclitaxel was sufficient to not only enhance the potency of cetuximab-mediated ADCP but also increase the extent of DLD1 clearance to twofold (Fig. 1F). In addition, paclitaxel increased the effect of cetuximab-mediated ADCP on SW480 cells by nearly threefold (Fig. 1G).

Motivated by these findings, we asked whether paclitaxel could exhibit similar effects with other therapeutic antibodies. Our data showed that paclitaxel at the tested concentration only had minimal effects on Raji cell growth, but combining it with rituximab led to potent effects on eliminating Raji cells compared to rituximab alone (fig. S3B). Blockade of FcγRs diminished the effects of paclitaxel on rituximab-induced phagocytosis, confirming the role of paclitaxel in enhancing ADCP (fig. S3C). In addition, we showed that rituximab- and trastuzumab-mediated cancer cell clearance by human peripheral blood monocyte–derived macrophages was significantly enhanced when combined with paclitaxel (Fig. 1H). The expression of the target receptors on cancer cells—EGFR, CD20, or HER2—was not affected by paclitaxel treatment (fig. S3D). Together, we identified a role of paclitaxel in substantially enhancing the ADCP of a variety of cancer cells mediated by several commonly used therapeutic antibodies.

Paclitaxel combined with anticancer antibody elicits strong anticancer activity in vivo

The combinatorial effect of paclitaxel and anticancer antibodies was further examined in the in vivo xenotransplantation models. In our study, we used RAG2$^{-/-}\gamma c^{-/-}$ and NSG mice, which lack T, B, and NK cells but retain functional macrophages (*38*), making them excellent models for studying macrophage-dependent immunity against human cancer cells. The human NHL cell line Raji transduced with green fluorescent protein (GFP)–luciferase was subcutaneously engrafted into the RAG2$^{-/-}\gamma c^{-/-}$ mice. Twenty-one days after tumor implantation, a minimal amount of paclitaxel (50 μg/kg) was administered locally through intratumoral injection and rituximab (7.5 mg/kg) was given intravenously twice every week (Fig. 2A). We found that either agent slowed the progression of tumors, whereas the combination almost completely eliminated the tumors in most mice (Fig. 2B and fig. S4, A and B), indicating a strong synergism between the drugs.

Next, we validated the efficacy of the combinatory treatment in two additional preclinical models. In these models, clinical-grade nanoparticle albumin–bound (nab) paclitaxel, which was indicated by clinical evidence as being better tolerated than solvent (Cremophor EL)–based paclitaxel (*39*, *40*), was used for intravenous treatment.

In the first model, Raji cells were intravenously injected into RAG2$^{-/-}\gamma c^{-/-}$ mice. At day 10 after engraftment, when lymphoma cells were clearly disseminated into the bone marrow compartment, the mice were treated with nab-paclitaxel (50 mg/kg) followed by one dose of rituximab every week (day 11 for the first dose of rituximab) for a total of 4 weeks (Fig. 2C). We showed that the combination nearly entirely controlled the disease progression in the period of treatment (Fig. 2D). As a direct comparison, rituximab alone produced minimal efficacy in this model (Fig. 2D), likely due to the late start of treatment, which mimicked the impact of tumor burden on rituximab efficacy in human patients with late-stage cancer (*23*, *24*). As a result, the combination significantly prolonged the survival of mice (Fig. 2E). The combination did not lead to body weight loss during the treatment period (Fig. 2F), indicating that the mice tolerated this dose regimen well.

In a second model of aggressive peritoneal colorectal cancer disease, SW480 cells expressing GFP-luciferase were intraperitoneally injected into the NSG mice. Nab-paclitaxel was used at 50 mg/kg, and this clinically relevant dose of paclitaxel was able to effectively promote antibody efficacy while being well tolerated. We showed that the combination of nab-paclitaxel and cetuximab significantly reduced the tumor burden (Fig. 2G and fig. S4C), highlighting the synergism between these two agents.

Paclitaxel enhances anticancer antibody efficacy by stimulating the phagocytic ability of macrophages

We next sought to understand the mechanisms underlying the strong synergism between paclitaxel and therapeutic antibodies. We reasoned that paclitaxel may act on either cancer cells or macrophages to stimulate the efficacy of antibodies. To investigate this, we pretreated either macrophages or DLD1 cells with paclitaxel and examined them in phagocytosis assays with nontreated DLD1 or

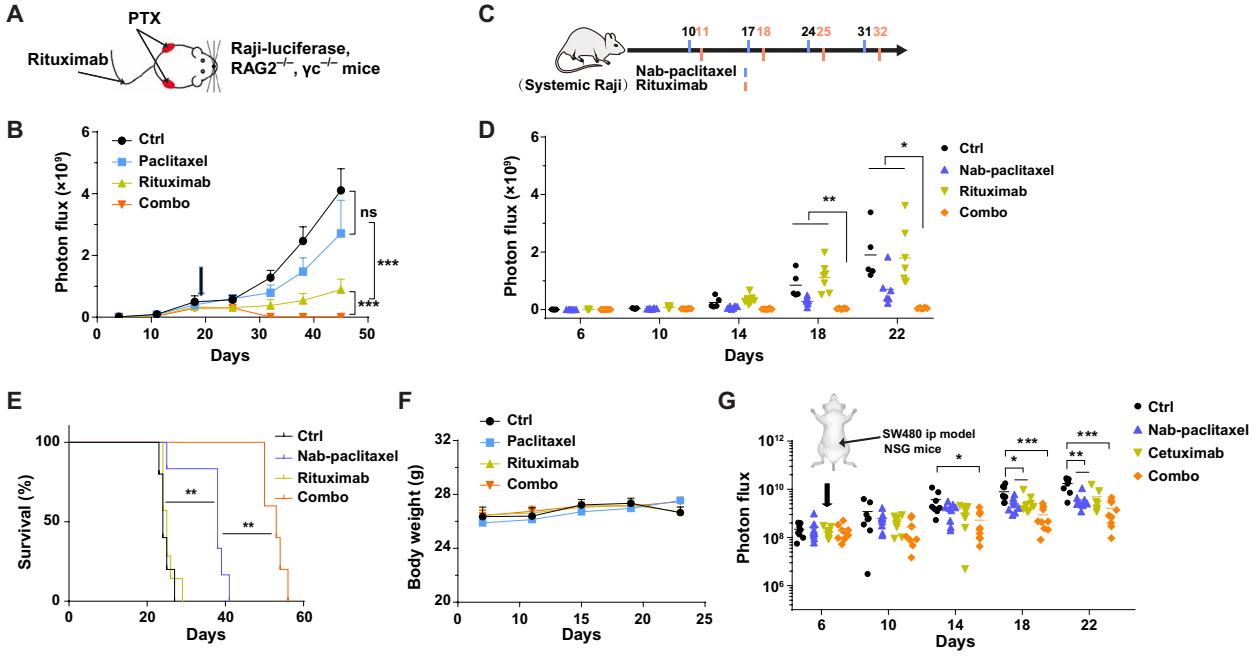

Fig. 2. Paclitaxel combined with anticancer antibody elicits strong anticancer activity in vivo. (**A**) Schematic showing the treatment strategy of the subcutaneous Raji models. PTX, paclitaxel. (**B**) Growth of tumors derived by Raji cells in RAG2$^{-/-}\gamma c^{-/-}$ mice. Mice subcutaneously engrafted with Raji cells were treated with phosphate-buffered saline (PBS), rituximab, paclitaxel, or a combination of rituximab and paclitaxel. Tumor growth was measured by bioluminescence imaging. $n = 12$; ***$P < 0.001$ (log-linear regression analysis). (**C**) Schematic showing the treatment strategy of the systemic Raji model. (**D**) Growth of tumors derived by Raji cells through intravenous injection into RAG2$^{-/-}\gamma c^{-/-}$ mice. Tumor signals were determined by bioluminescence imaging. $n = 5$ to 7; *$P < 0.05$ and **$P < 0.01$ (one-way ANOVA). (**E**) Survival analysis of animals in (D). $n = 5$ to 7; **$P < 0.01$ [log-rank (Mantel-Cox) test]. (**F**) Body weight analysis of animals in (D). $n = 5$ to 7. (**G**) Growth of tumors derived by SW480 cells in NSG mice. Mice intraperitoneally engrafted with SW480 cells were treated with PBS, cetuximab, nab-paclitaxel, or a combination of cetuximab and nab-paclitaxel. Tumor growth was measured by bioluminescence imaging. $n = 7$ to 9; *$P < 0.05$, **$P < 0.01$, and ***$P < 0.001$ (one-way ANOVA).

macrophages, respectively, in the presence of cetuximab (Fig. 3A). We showed that paclitaxel-treated DLD1 cells displayed a similar tendency to phagocytosis compared to their untreated counterparts (Fig. 3B). In contrast, paclitaxel-treated macrophages strongly potentiated the effect of cetuximab (Fig. 3B), indicating that paclitaxel directly stimulated the phagocytic ability of macrophages. This was further supported by the flow cytometry–based assay examining the percentages of macrophages phagocytosing cancer cells. We showed that paclitaxel pretreatment of macrophages largely boosted cetuximab-induced phagocytosis of DLD1 or SW480 cells, and phagocytosis of Raji cells by rituximab (Fig. 3, C to E). In an additional experiment, we examined phagocytosis with microscopic visualization, which revealed much higher numbers of macrophages in paclitaxel-pretreated group phagocytosing cancer cells as compared to vehicle-treated macrophages in the presence of anticancer antibodies (Fig. 3F and fig. S5A).

The role of paclitaxel in boosting ADCP of cancer cells was further examined in in vivo and ex vivo animal models. First, an adoptive transfer of macrophages was performed in RAG2$^{-/-}\gamma c^{-/-}$ mice subcutaneously engrafted with Raji cells. The mice received either vehicle-treated or paclitaxel-treated macrophages through intratumoral injection. Rituximab was intravenously administered to both groups of mice immediately after the adoptive transfer of macrophages (Fig. 3G). We showed that paclitaxel-treated macrophages exhibited a much stronger effect on delaying tumor progression in the presence of rituximab than the vehicle-treated counterparts (Fig. 3G). Next, we performed an ex vivo phagocytosis assay with femur macrophages. Mice were given vehicle or nab-paclitaxel treatment, after which femur bone marrow cells were obtained and subjected to phagocytosis assays with Raji cells. We found that femur macrophages (CD45^{+}F4/80^{+}) from nab-paclitaxel–treated mice

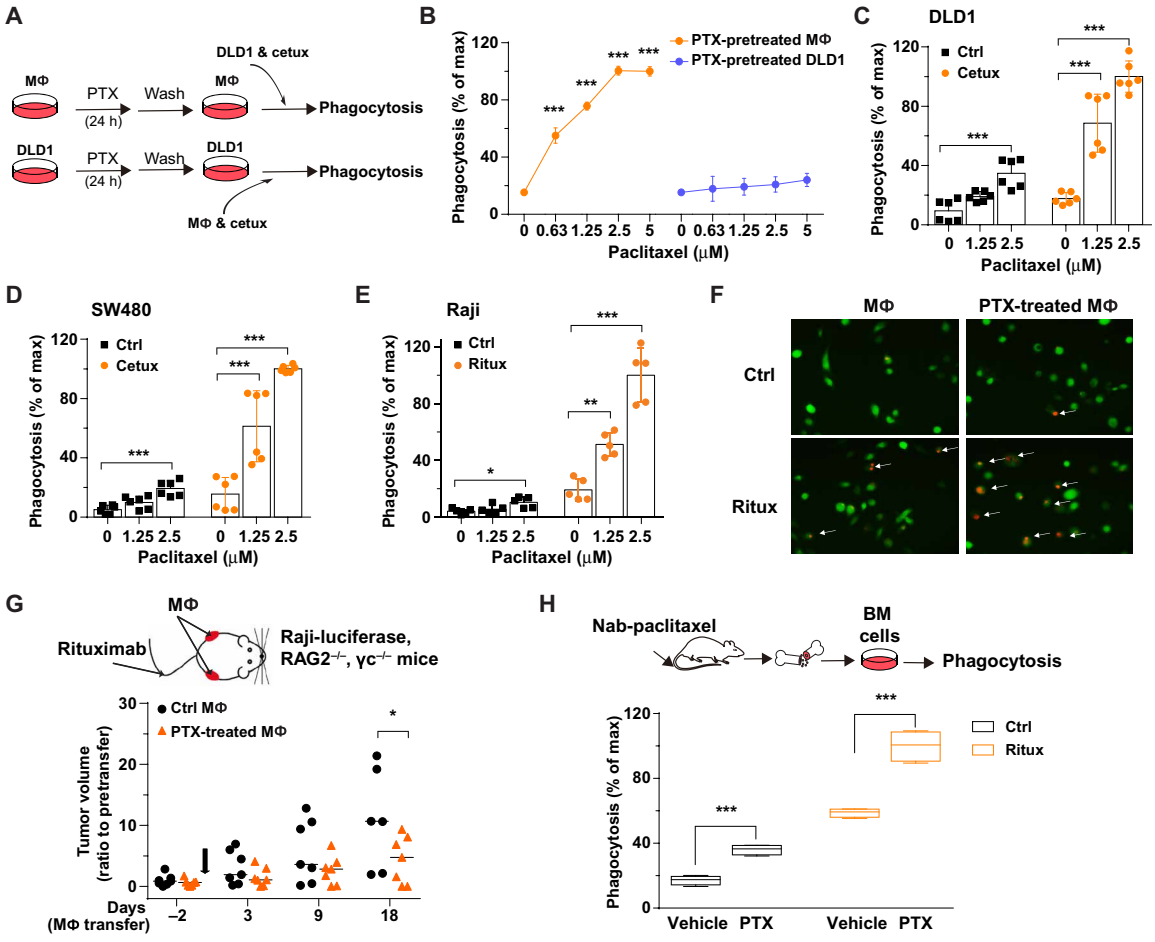

Fig. 3. Paclitaxel enhances anticancer antibody efficacy by stimulating the phagocytic ability of macrophages. (**A**) Schematic showing the experimental design to determine whether paclitaxel acted on cancer cells or macrophages (MΦ) to enhance anticancer antibody–mediated phagocytosis. (**B**) Paclitaxel-pretreated macrophages, but not DLD1 cells, exhibited enhanced phagocytosis in the presence of cetuximab, measured by a luminescence-based phagocytosis assay. $n = 4$; ***$P < 0.001$ (one-way ANOVA). An in vitro flow cytometry–based phagocytosis assay with DLD1 cells (**C**), SW480 cells (**D**), or Raji cells (**E**) as target cells. BMDMs pretreated with DMSO or paclitaxel were used for the assay. Phagocytosis assay was performed in the presence of cetuximab (DLD1 and SW480 cells) or rituximab (Raji cells). Phagocytosis was normalized to the maximal response in the experiments. Each group was compared with the control group (0 μM paclitaxel). $n = 5$ to 6; *$P < 0.05$, **$P < 0.01$, and ***$P < 0.001$ (one-way ANOVA). (**F**) Microscopy-based phagocytosis assay with Raji cells as target cells. Mouse BMDMs (green) were stained with calcein green, and Raji cells (red) were labeled with pHrodo Red. Representative fluorescence microscopic images of two independent experiments. Arrows indicated the macrophages (double colors) that phagocytosed cancer cells. (**G**) Adoptive transfer of paclitaxel-treated macrophages enhanced the efficacy of rituximab. RAG2$^{-/-}\gamma c^{-/-}$ mice subcutaneously engrafted with Raji cells received intratumoral injections of DMSO-treated (Ctrl) or paclitaxel-treated macrophages. Rituximab was given through intravenous injection. $n = 7$; *$P < 0.05$ (t test). (**H**) Femur macrophages from nab-paclitaxel–treated mice demonstrated higher phagocytic ability toward Raji cells in the presence of rituximab. BM, bone marrow. $n = 4$; ***$P < 0.001$ (t test).

demonstrated a significant increase in the ability of phagocytosing Raji cells in the presence of rituximab, as compared to the vehicle-treated counterparts (Fig. 3H and fig. S5B). Last, we examined the ADCP of cancer cells by TAMs. RAG2$^{-/-}\gamma c^{-/-}$ mice were engrafted with SW480 cells expressing GFP-luciferase subcutaneously and treated with control vehicle, cetuximab, nab-paclitaxel, or a combination of cetuximab and nab-paclitaxel. The tumors were collected and subjected to fluorescence-activated cell sorting (FACS) analysis. We showed that TAMs from mice treated with a combination of cetuximab and nab-paclitaxel demonstrated significantly enhanced phagocytosis against cancer cells (fig. S5, C and D). Together, our data from a set of in vitro and in vivo models provided compelling evidence that paclitaxel enhanced anticancer antibody efficacy by stimulating the phagocytic ability of macrophages.

Paclitaxel stimulates macrophage polarization toward the state with an enhanced phagocytic ability

Next, we sought to explore the functional phenotypes of macrophages. We showed that paclitaxel treatment induced M1 differentiation as reflected by the up-regulation of major histocompatibility complex II (MHCII) and down-regulation of CD206 in BMDMs (Fig. 4A). We then performed RNA sequencing on vehicle- or paclitaxel-treated BMDMs (Fig. 4B). Up-regulation of a group of M1 macrophage–associated markers indicated an M1-like polarization of macrophages by paclitaxel (Fig. 4C). This is consistent with our findings that macrophages polarized toward an M1-like phenotype had stronger ADCP ability against cancer cells, as compared to M0 macrophages, while M2-polarized macrophages demonstrated compromised phagocytosis ability toward cancer cells (Fig. 4D and

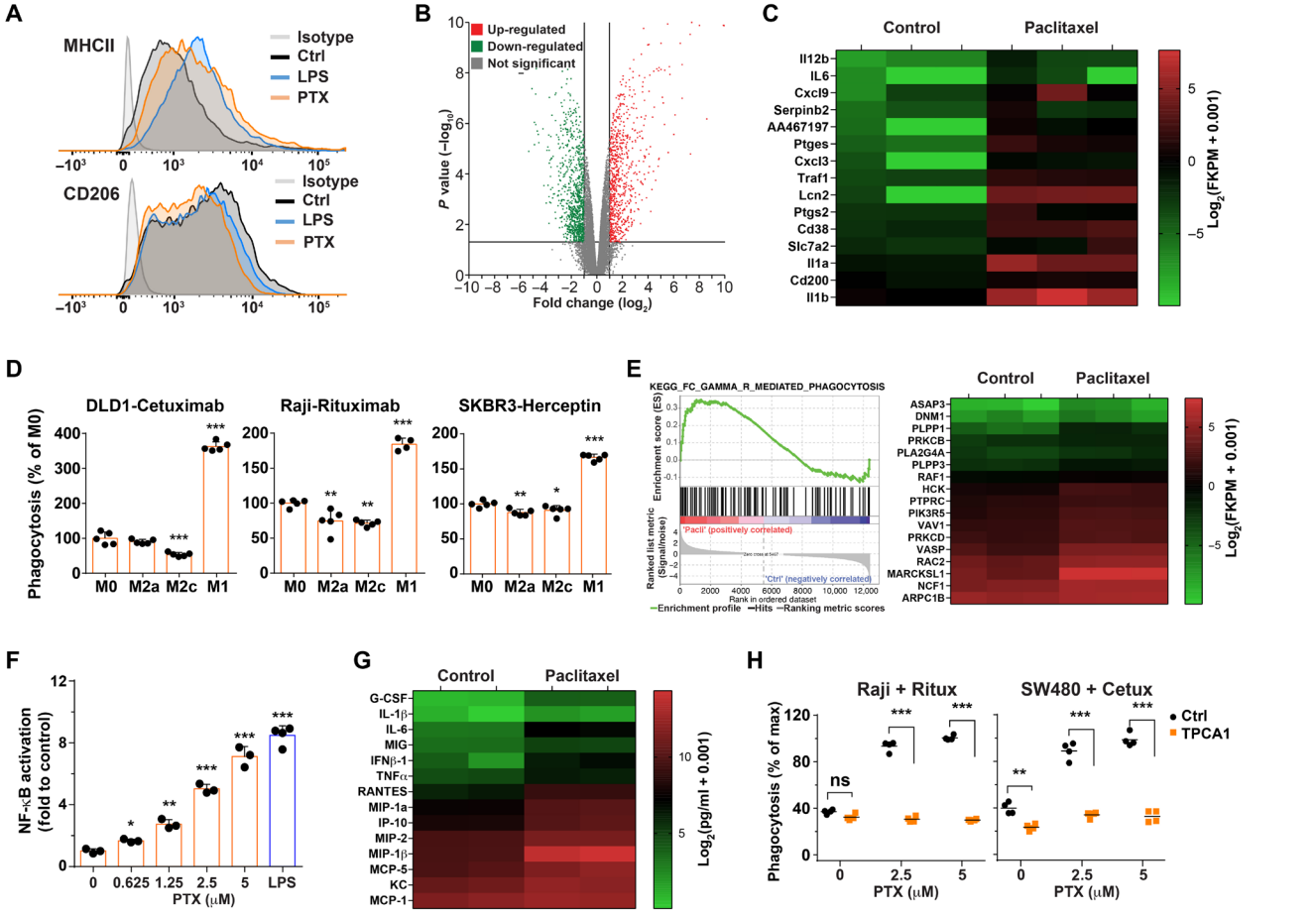

Fig. 4. Paclitaxel stimulates macrophage polarization toward the state with an enhanced phagocytic ability. (**A**) Representative FACS plots showing the expression of MHCII (top) and CD206 (bottom) on BMDMs stimulated with paclitaxel or DMSO (control). Representative FACS plots of three independent experiments. (**B**) Volcano plot showing differentially expressed genes in DMSO-treated and paclitaxel-treated BMDMs. Genes with a *P* value of <0.05 and a fold change of >2 were considered significantly up-regulated or down-regulated. BMDMs were generated from three individual BALB/c mice for triplicated samples. (**C**) Heatmap of gene expression profile by RNA sequencing showing the up-regulation of M1-like gene signature. $n = 3$. (**D**) An in vitro flow cytometry–based phagocytosis assay with polarized BMDMs showing impaired phagocytic ability of M2-like macrophages and increased phagocytic ability of M1-like macrophages. $n = 5$; $^{*}P < 0.05$, $^{**}P < 0.01$, and $^{***}P < 0.001$ (one-way ANOVA). (**E**) KEGG (Kyoto Encyclopedia of Genes and Genomes) enrichment analysis showing the up-regulation of FcγR-mediated phagocytic pathway upon paclitaxel treatment (left). A heatmap of gene expression profile by RNA sequencing showing the up-regulation of phagocytosis-related gene signature in paclitaxel-treated BMDMs (right). $n = 3$. (**F**) Activation of nuclear factor κB (NF-κB) signaling pathway, as measured by an NF-κB reporter system. RAW264.7 macrophages were stimulated with various concentrations of paclitaxel or lipopolysaccharide (LPS) (1 ng/ml) (positive control). Unstimulated RAW264.7 cells acted as a negative control. Each group was compared with the control group (0 μM paclitaxel). $n = 3$ to 4; $^{*}P < 0.05$, $^{**}P < 0.01$, and $^{***}P < 0.001$ (one-way ANOVA). (**G**) Measurement of cytokine and chemokine secretion profile of BMDMs treated with DMSO (control) or paclitaxel by a Luminex assay. Experiments were performed in duplicate. (**H**) In vitro flow cytometry–based phagocytosis assay with Raji or SW480 cells as target cells. BMDMs were pretreated with various concentrations of paclitaxel in the absence or presence of TPCA1 or antibodies. Phagocytosis was normalized to the maximal response in the experiments. $n = 4$; $^{**}P < 0.01$ and $^{***}P < 0.001$ (one-way ANOVA).

fig. S6, A to C). Consistently, gene set enrichment analysis (GSEA) revealed that paclitaxel treatment induced a pro-phagocytic transcriptional response in BMDMs, with a significant enrichment of genes involved in the FcγR-mediated phagocytosis pathways (Fig. 4E).

Using RAW264.7 cells, a macrophage cell line that was engineered to report nuclear factor κB (NF-κB) activity, we showed a significant activation of NF-κB pathway upon paclitaxel treatment (Fig. 4F), along with the production of NF-κB pathway-controlled proinflammatory cytokines and chemokines such as IL-1β (interleukin-1β), IL-6, monocyte chemoattractant protein-1 (MCP1), and TNFα (tumor necrosis factor α) (Fig. 4G). Analysis of the BMDM model demonstrated enhanced phosphorylation of NF-κB (p65) and IκBα (inhibitor of NF-κBα) (fig. S7A) upon paclitaxel treatment. In addition, nuclear translocation of NF-κB was induced in BMDMs treated with paclitaxel, as demonstrated by examining the nuclear and cytosolic fractions of macrophages (fig. S7B) and microscopic visualization of NF-κB subcellular localization in macrophages (fig. S7C). Consistently, paclitaxel-mediated up-regulation of NF-κB activity (fig. S7D) and enhanced phagocytic ability of macrophages (Fig. 4H) were largely attenuated by TPCA1, a specific inhibitor of NF-κB pathway, indicating that the activation of NF-κB pathway is critical for paclitaxel-induced polarization of macrophages.

CSF1R down-regulation contributes to the enhanced phagocytic ability of macrophages by paclitaxel

Cell surface receptors play key roles in regulating immune cell function by binding to their ligands and transducing cellular signaling (*41*, *42*). We decided to investigate whether and how macrophage surface proteins may involve in paclitaxel-induced enhancement in the phagocytic ability of macrophages. We examined the effects of paclitaxel treatment on the expression of nine surface proteins including well-known macrophage surface markers and phagocytosis checkpoint proteins (Fig. 5A and fig. S8) (*43*). Our results revealed an up-regulation of CD86 and TLR2 upon paclitaxel treatment, consistent with the M1 differentiation induced by paclitaxel. We also observed a slight up-regulation of PD1 on macrophages, the deletion of which was previously shown to induce the phagocytosis of PDL1^{+} cancer cells (*44*). Among the surface markers, when macrophages were treated with paclitaxel, F4/80 was up-regulated, while CSF1R expression was significantly down-regulated (Fig. 5, A and B, and fig. S8). CSF1R is important for the development and differentiation of macrophages and has emerged as an important therapeutic target in recent years (*45*, *46*). Consistent with several previous studies (*47*, *48*), our analysis with public databases suggested that lower expression of CSF1R in tumors can serve as a predictor of the beneficial outcome of patients in a broad spectrum of malignancies (fig. S9), suggesting a possible antitumor role of TAMs with low CSF1R expression.

This inspired us to examine a possible link of causality between CSF1R down-regulation and paclitaxel-stimulated enhancement of macrophage phagocytosis. BMDMs were treated with small interfering RNA (siRNA) to knock down CSF1R expression and then used for phagocytosis assays with therapeutic antibodies. We showed that CSF1R knockdown led to an enhancement of phagocytosis of DLD1 cells or Raji cells to a level similar to that induced by knocking down the phagocytosis checkpoint Sirpα in the presence of cetuximab or rituximab (Fig. 5C and fig. S10, A to C). To further evaluate the role of CSF1R in mediating ADCP, we performed an ex vivo experiment in which we knocked down CSF1R with CRISPR-mediated gene editing by transducing single-guide RNAs (sgRNAs) targeting CSF1R in BMDMs from CRISPR-Cas9 knockin mouse model [Gt(ROSA)26Sor$^{em1.1(CAG\text{-}cas9*,\text{-}EGFP)Rsky}$] (*49*). Consistently, CSF1R knockdown in macrophages exhibited a much stronger effect on

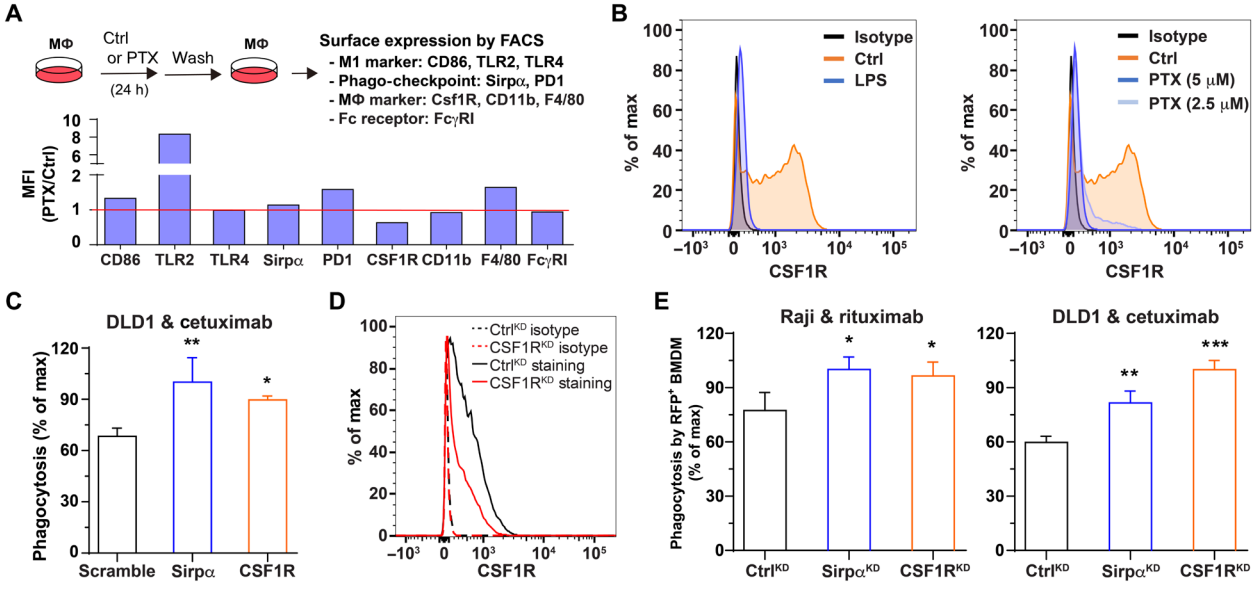

Fig. 5. CSF1R down-regulation contributes to the enhanced phagocytic ability of macrophages by paclitaxel. (**A**) Surface expression of nine macrophage surface markers and phagocytosis checkpoint proteins upon paclitaxel stimulation. (**B**) Paclitaxel at various concentrations and M1 macrophage polarization inducer LPS down-regulated macrophage cell surface CSF1R. Representative FACS plots of three independent experiments. (**C**) Knockdown of CSF1R with small interfering RNA (siRNA) enhanced the phagocytic ability of BMDMs toward DLD1 cells in the presence of cetuximab. $n = 3$; $^{*}P < 0.05$ and $^{**}P < 0.01$ (one-way ANOVA). (**D**) CSF1R knockdown by CRISPR technology in primary BMDMs from Cas9 knockin mice transduced with a single-guide RNA (sgRNA) targeting CSF1R. (**E**) CSF1R knockdown increased the phagocytic ability of BMDMs toward Raji cells (in the presence of rituximab) and DLD1 cells (in the presence of cetuximab). BMDMs from Cas9 knockin mice were transduced with nontargeting sgRNA (control), Sirpα sgRNA (positive control), or CSF1R sgRNA. $n = 4$ to 5; $^{*}P < 0.05$, $^{**}P < 0.01$, and $^{***}P < 0.001$ (one-way ANOVA).

enhancing ADCP compared to the nontargeting control (Fig. 5, D and E). These data suggested an unprecedented role of CSF1R in regulating macrophage phagocytosis. CSF1R expression inversely correlated with the response of cetuximab response in colorectal cancer patients (fig. S10D). We found that treatment of macrophages with an anti-CSF1R antibody or inhibitors targeting the tyrosine kinase domain of CSF1R (*50*, *51*), or suppression of CSF1 in DLD1 cells, showed no effect on ADCP of cancer cells (fig. S10, E to I), suggesting that CSF1R may play an inhibitory role independently of the CSF1-CSF1R signaling axis and does not rely on its intracellular tyrosine kinase activity.

Paclitaxel potentiates the efficacy of cetuximab in a patient-derived xenograft model of colorectal cancer

Patient-derived xenograft (PDX) models are considered as valuable preclinical models evaluating cancer treatment approaches; thus, we sought to further investigate the therapeutic potential of the combinatorial regimen with PDX models of colorectal cancer. We used a PDX model with KRAS mutant while expressing human EGFR (fig. S11A). Upon engraftment, the mice were treated with either nab-paclitaxel, cetuximab, or a combination of the two, and tumor growth was monitored regularly. Our results showed that cetuximab alone slowed cancer progression of this PDX (Fig. 6A), whereas combination with nab-paclitaxel largely enhanced the effect of cetuximab in suppressing the growth of PDX tumors without affecting the body weight of the treated mice (Fig. 6, A and B, and fig. S11B). Thus, nab-paclitaxel also showed a synergistic effect with monoclonal antibody cetuximab on inhibiting the development of colorectal cancer PDX tumors.

Next, the PDX tumors from the control group and nab-paclitaxel group were collected and a single-cell suspension was prepared for the analysis of TAMs. Paclitaxel treatment led to an enrichment of TAMs in the tumor mass (Fig. 6C). Consistently, an up-regulation of MHCII and inducible nitric oxide synthase (iNOS) and a down-regulation of CD206 expression, as well as increased phosphorylation of IκBα, were observed in TAMs from nab-paclitaxel–treated mice, indicating an increase of M1 polarization (Fig. 6D and fig. S11, C to E).

Together, we propose a model (Fig. 6E) to summarize our findings on stimulating macrophage ADCP to enhance the efficacy of therapeutic antibodies for the treatment of malignant diseases. Specifically, inefficient ADCP by TAMs, especially those in bulky diseases such as solid tumors, may therefore limit the therapeutic efficacy of monoclonal antibodies. Paclitaxel stimulates TAM-mediated phagocytosis by inducing M1 polarization in an NF-κB pathway–dependent manner and substantially boosts antibody efficacy. Reduction of CSF1R from macrophage cell surface also contributes to the enhanced phagocytosis of cancer cells induced by monoclonal antibodies.

DISCUSSION

The unique feature of anticancer monoclonal antibodies in their specificity and ability to elicit immune response makes these "magic bullets" indispensable in the arsenal fighting against human cancers. Here, we demonstrated macrophage phagocytosis as a key mechanism underlying the anticancer effect of therapeutic antibodies. The process is amendable by chemotherapeutic drugs such as paclitaxel, providing a potential combinatorial strategy to enhance

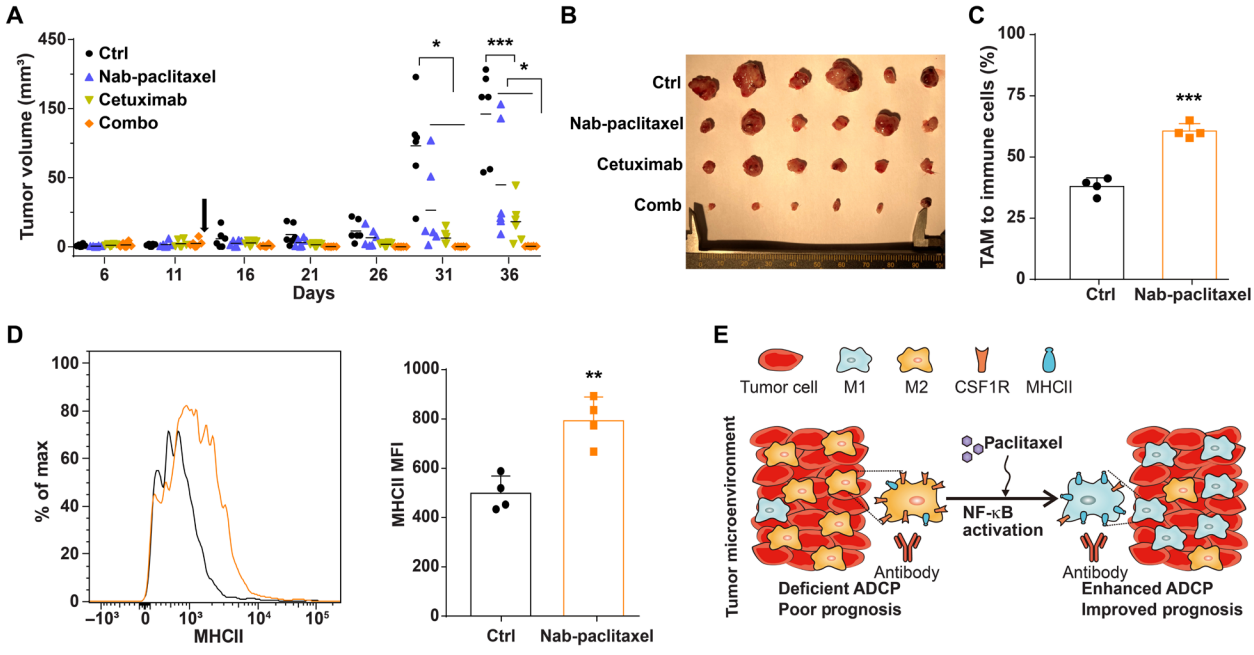

Fig. 6. Nab-paclitaxel potentiates the efficacy of cetuximab in a PDX model of colorectal cancer. (**A**) Growth of tumors developed by PDX colorectal cancer cells in RAG2$^{-/-}$γc$^{-/-}$ mice. Mice subcutaneously engrafted with PDX tumors were treated with control vehicle, cetuximab, nab-paclitaxel, or a combination of cetuximab and nab-paclitaxel. Tumor growth was monitored by regular measurement of tumor sizes. $n = 6$; *$P < 0.05$ and ***$P < 0.001$ (one-way ANOVA). (**B**) Representative tumor images on day 36 after engraftment. (**C**) Proportion of F4/80$^+$ TAMs in CD45$^+$ immune cells, in tumors developed by PDX colorectal cancer in RAG2$^{-/-}$γc$^{-/-}$ mice. Mice were treated with vehicle or nab-paclitaxel. $n = 4$; ***$P < 0.001$ (*t* test). (**D**) Representative FACS plots and mean fluorescent intensity (MFI) of MHCII expression on TAMs from RAG2$^{-/-}$γc$^{-/-}$ mice engrafted with the PDX colorectal cancer cells. Mice were treated with vehicle or nab-paclitaxel. $n = 4$; **$P < 0.01$ (*t* test). (**E**) Schematic showing that paclitaxel enhances macrophage-mediated phagocytosis of cancer cells in the presence of therapeutic antibodies.

the clinical benefit and/or overcome clinical resistance of anticancer antibodies.

Despite the reported role of TAMs in mediating anticancer activity of monoclonal antibodies for hemopoietic malignancies (*21*, *22*, *52*), whether this stands in solid tumors remains unclear. For example, previous clinical studies showed that bypassing EGFR signaling with KRAS mutation in colorectal cancer patients led to notable resistance to cetuximab treatment (*37*, *53*). This KRAS mutation–induced resistance to cetuximab was recaptured with multiple colorectal cancer cell lines in our study; however, the inclusion of macrophages renders these tumor cells responsive to cetuximab treatment and the effectiveness is well reflected by the surface abundance of EGFR. Consistent with our analysis, several clinical studies also indicate the correlation of EGFR surface level with the efficacy of cetuximab in colorectal cancer and SCCHN patients regardless of their KRAS status (*54*, *55*). These indicated a process of ADCP, which was confirmed by our phagocytosis assays with both mouse and human primary macrophages. Moreover, we found a complete loss of efficacy when rituximab is administered at relatively late stages of NHL disease, while early administration of cetuximab induced notable macrophage-dependent clearance of KRAS mutant SW480 cells. These results reinforced the notion that tumor progression may program TAMs toward a phenotype with an impaired phagocytic ability (*56*). Therefore, we propose several possible explanations for the limited ADCP reported in solid tumors: (i) Antibodies may not be able to sufficiently infiltrate into solid tumors (*57*), and therefore, a threshold to initiate ADCP may not be achieved in some patients; (ii) the targeted antigen level on solid tumors is normally lower than those on hemopoietic tumors (*58*), and as a result, there may be an intrinsic limitation on the extent of ADCP in these tumors; and (iii) the more established TME in solid tumors when starting antibody treatment may consist of TAMs with more severely impaired phagocytic ability.

Our demonstration of macrophage phagocytosis as a key mechanism in eliciting the anticancer effect of monoclonal antibodies suggested that these cells may be a feasible target to augment the antibodies' response and overcome their resistance. In light of a shortage of proper screening platforms for identifying phagocytosis modulators, we established an extremely versatile coculturing system able to accurately quantify long-term phagocytosis rate by measuring the luminescence signals from remaining surviving cancer cells. While we screened the currently FDA-approved anticancer small molecules aiming to identify candidates readily translatable to clinical benefits, this platform is also applicable to experiments screening any other chemical or genetic modulators for macrophage phagocytosis of living cancer cells. The screen enabled us to identify several promising small molecules potentially augmenting antibody effectiveness in the presence of macrophages. Among them, imiquimod, a TLR9 agonist, is actively under clinical investigation combined with pembrolizumab in treating patients with stage IIIB-IV melanoma (NCT03276832) and locally advanced unresectable or cutaneous metastatic breast cancer (NCT03982004). Cabazitaxel was recently found to be able to enhance CD47 blocking antibody efficacy in triple-negative breast cancer by enhancing macrophage phagocytosis (*59*). These together suggest the excellent reliability and applicability of our novel phagocytosis screen platform. In contrast, numerous kinase inhibitors, particularly those bearing inhibitory activity on Src, Btk, and Akt, were found to inhibit the efficacy of cetuximab. Because we used KRAS mutated cancer cells for the screen, this effect is likely not due to their effect on cetuximab-mediated inhibition of EGFR signaling, but rather due to the inhibition of macrophage phagocytosis given their roles in mediating macrophage function (*60*, *61*). This observation also reinforced the concern raised by Sharma and Allison (*62*) regarding the potential counteracting effect of certain kinase inhibitory drugs to immunotherapies when combining these agents in clinical use.

The immunomodulatory effects of paclitaxel have been supported by the fact that it is so far the only chemotherapeutic drug approved to be combined with atezolizumab for triple-negative breast cancer (TNBC), a type of tumor-bearing highly immunosuppressive TME (*63*). Paclitaxel emerged as a top hit in our screen and elicited synergistic antitumor effects when combined with therapeutic antibodies. Several layers of experiments were performed to demonstrate its stimulatory effect on macrophages: (i) Pretreated macrophages elicited much stronger anticancer activity in the presence of anticancer antibodies in phagocytosis and adoptive transfer assays; (ii) with mice only bearing functional macrophages, a nontoxic level of paclitaxel was sufficient to augment the efficacy of rituximab; and (iii) with the same type of mice, paclitaxel treatment was also able to resensitize the response to rituximab, which had otherwise completely lost its anticancer activity. Previous studies demonstrate that macrophages are highly tolerant to paclitaxel toxicity (*64*), which excludes the possibility that the clinical dose of paclitaxel harms TAMs and therefore limits the efficacy of therapeutic antibodies. Consistently, our study with a clinically relevant dose of paclitaxel nearly entirely controlled the tumor progression when combined with rituximab, and substantially slowed the growth of human colorectal cancer PDX when combined with cetuximab.

In agreement with a recent finding (*64*), paclitaxel induced an M1 phenotype of macrophages. The conversion to M1 macrophages largely enhanced antibody-induced phagocytosis, a phenomenon distinct from efferocytosis of apoptotic cancer cells, which largely relies on M2 macrophages (*65*). Because of our observation that macrophages were the main target cells of paclitaxel in terms of stimulating phagocytosis, we focused on identifying the signaling pathways in macrophages responsible for this effect. We uncovered that this occurred via an NF-κB–dependent manner. That is, the blockade of the NF-κB pathway not only abolished the M1 TAM polarization but also inhibited their phagocytic capability, indicating that activating NF-κB signaling may be a strategy to potentiate macrophage response to monoclonal antibodies. NF-κB activation is believed to transmit survival signals in cancer cells, and therefore, its sustaining activation may lead to resistance to anticancer drugs (*66*). This again reinforces how the inhibition of cancer cell survival signaling may cause distinct outcomes in immune cells and may potentially jeopardize the efficacy of immunotherapy when doing combination therapies in clinical.

TAM abundance within the TME has been repeatedly demonstrated to be correlated with a poor patient prognosis across different malignancies (*67*, *68*). Because of this, methods of targeting TAMs have been pioneered, such as the blockade of CSF1R in an effort to deplete TAMs (*45*). Unfortunately, none of these agents has shown acceptable clinical efficacy in human patients as a monotherapy. Emerging evidence in recent years has highlighted the important role of surface proteins in regulating immune cell functions, exemplified by Sirpα on macrophages (*69*), CTLA4 on T cells (*70*), etc. This led us to examine whether paclitaxel could exert its effect by regulating the abundance of macrophage surface proteins. Most of the proteins we examined remained unaltered upon paclitaxel treatment, but we

noticed an up-regulation of MHCII on paclitaxel-treated macrophages. This not only indicates an M1 polarization state but also implies a possibly enhanced capacity for antigen presentation upon paclitaxel treatment, which warrants further investigation in immunocompetent settings. In contrast, paclitaxel stimulation led to a significant reduction of CSF1R in macrophages. In addition to its critical roles in TAM recruitment, polarization, and survival (*71*), CSF1R has been reported to be involved in phagocytosis in previous studies. An induction of cancer cell phagocytosis was achieved by dual-inhibitor–loaded nanoparticles to simultaneously block the "don't eat me" signal CD47 and target the CSF1-CSF1R pathway for repolarizing TAMs. In addition, the inhibitor PLX5622 that targeted the tyrosine kinase activity of CSF1R in macrophages inhibited IL-1β expression and suppressed phagocytosis of *Escherichia coli* bioparticles (*72*, *73*). Therefore, we attempted to investigate whether the down-regulation of CSF1R may affect macrophage phagocytosis by knocking down CSF1R from mature macrophages with siRNA or CRISPR-Cas9 technology. Unexpectedly, a knockdown of CSF1R with both methods significantly enhanced antibody-mediated phagocytosis of cancer cells. In agreement, numerous clinical studies have found that lower expression of CSF1R in tumor tissues correlates with not only the efficacy of therapeutic antibodies such as cetuximab but also the reduced overall mortality in different malignancies (*47*, *48*, *74*). Ongoing clinical trials are evaluating the effects of blocking the CSF1-CSF1R interaction and/or targeting the tyrosine kinase activity of CSF1R for TAM depletion or polarization for cancer treatment (*45*). Our results suggested a potential CSF1-independent role of CSF1R in regulating ADCP, and we showed that blockade of its intracellular tyrosine kinase domain showed minimal effects on ADCP of cancer cells. In addition, it is likely that CSF1R down-regulation may induce a proinflammatory response in macrophages, as suggested by the observation of enhanced proinflammatory IFNγ (interferon-γ) signaling in breast cancer patients with a low CSF1R expression (*75*). Together, further clarification of the underlying mechanisms of CSF1R in negatively regulating ADCP and the development of strategies to reduce CSF1R expression on macrophages may serve as a novel macrophage-targeting approach to treat cancer.

In conclusion, our work demonstrates an essential role of macrophages in mediating the efficacy of therapeutic antibodies and provides a rational strategy of combining paclitaxel and antibody drugs for the therapy of malignant diseases. In addition, our study identifies a role of CSF1R in regulating macrophage phagocytosis. Further examination of the regulatory effect of CSF1R will not only shed light on the understanding of macrophage physiology but also facilitate the development of novel cancer therapies.

MATERIALS AND METHODS

Mice

BALB/c, NOD.Cg-Prkdcscid Il2rgtm1Wjl/SzJ (NSG), Gt(ROSA)26Sor(em1.1(CAG-cas9*,-EGFP)Rsky)/B6(C)J, and RAG2$^{-/-}$γc$^{-/-}$ BALB/c mice were bred in the Animal Resources Center at City of Hope Comprehensive Cancer Center. BALB/c, NSG, and Cas9 mice were purchased from The Jackson Laboratory. RAG2$^{-/-}$γc$^{-/-}$ BALB/c mouse strain was a gift from I. L. Weissman at Stanford University. All the procedures were approved by the Administrative Panel on Laboratory Animal Care at City of Hope Comprehensive Cancer Center.

Cell culture

SW480 and RAW264.7 cells were cultured in Dulbecco's modified Eagle medium (DMEM) (Gibco) supplemented with 10% fetal bovine serum (FBS) (Gibco) and 1% penicillin/streptomycin. DLD1, Raji, and SKBR3 cells were cultured in RPMI 1640 (Gibco) supplemented with 10% FBS (Gibco) and 1% penicillin/streptomycin. SCC9 cells were cultured in a 1:1 mixture of DMEM (Gibco) and Ham's F12 medium containing sodium bicarbonate (1.2 g/liter), 2.5 mM L-glutamine, 15 mM Hepes, and 0.5 mM sodium pyruvate supplemented with hydrocortisone (400 ng/ml), 10% FBS (Gibco), and 1% penicillin/streptomycin. All cell lines were purchased from the American Type Culture Collection and maintained at 37°C in a 5% CO_2 atmosphere. Large quantities of low-passage (below 3) cells were cryopreserved, and cells with passage numbers below 20 were used in this study. Mycoplasma examination was routinely performed every 2 months.

Analysis of clinical dataset

CSF1R gene expression data in the form of $\log_2$(fpkm-uq + 1) from primary tumors of BLCA TCGA Bladder Urothelial Carcinoma dataset, COAD TCGA Colon adenocarcinoma dataset, LUSC TCGA Lung squamous cell carcinoma dataset, STAD TCGA Stomach adenocarcinoma dataset, and THYM TCGA Thymoma dataset were acquired from UCSC Xena (https://xenabrowser.net/) and associated with patient survival. For analyzing the correlation of EGFR expression and patient response to cetuximab treatment, GSE65021 was used to retrieve the expression of EGFR and patient response data. For analyzing the correlation of CSF1R expression and patient response to cetuximab treatment, GSE5851 was used to retrieve the expression of Csf1R and patient response data. The data were plotted with GraphPad Prism (version 6), and statistical significance was assessed within the software.

Generation of primary macrophages

To generate mouse BMDMs, bone marrow cells were harvested from the femur and tibia of 6- to 12-week-old BALB/c mice as previously described (*76*). After the red blood cells were lysed by Ammonium Chloride Potassium (ACK) buffer for 2 min, the bone marrow cells were filtered through a 70-μm strainer, washed twice with DMEM supplemented with 10% FBS, and cultured at 37°C in Iscove's modified Dulbecco's medium (IMDM) supplemented with 10% FBS and murine macrophage colony-stimulating factor (MCSF) (10 ng/ml) for 6 to 8 days to differentiate into macrophages.

To generate human peripheral blood monocyte–derived macrophages, human peripheral blood was obtained from the blood center at City of Hope Helford Clinical Research Hospital. CD14$^+$ monocytes were enriched by magnetic-activated cell sorting with CD14 MicroBeads (Miltenyi Biotec) and subsequently cultured at 37°C in IMDM with 10% human serum (Omega Scientific) for 6 to 8 days to differentiate into macrophages.

Phagocytosis assay

Phagocytosis rate was evaluated with mouse BMDMs or human peripheral blood monocyte–derived macrophages. Target cancer cells were either GFP-expressing or labeled with CellTrace-Green. For CellTrace-Green labeling, cells were incubated with 200 nM CellTrace-Green in phosphate-buffered saline (PBS) at 37°C for 20 min and washed twice with DMEM supplemented with 10% FBS. Macrophages were harvested using TrypLE and scrappers, cocultured

with target cancer cells in the presence of antibodies or immunoglobulin G (IgG) control (BioLegend), and incubated for 2 hours at 37°C. Before flow cytometry analysis, F4/80 antibody (BioLegend) conjugated with phycoerythrin (PE)–Cy7 was used to label macrophages. Phagocytosis was quantified as the percentage of macrophages that phagocytosed cancer cells during the incubation, namely, the ratio of $GFP^+PE\text{-}Cy7^+$ or $CellTrace\text{-}Green^+PE\text{-}Cy7^+$ cells to $PE\text{-}Cy7^+$ cells. For phagocytosis assays with Cas9 knockin mouse BMDMs, we quantified the phagocytosis mediated by RFP^+ macrophages by flow cytometry. Red fluorescent protein (RFP) expression indicated the transduction of macrophages with sgRNAs. Phagocytosis was quantified as the ratio of GFP^+RFP^+ or $CellTrace\text{-}Green^+RFP^+$ cells to RFP^+ cells. The phagocytosis index was normalized to the maximal response in every experiment.

For long-term phagocytosis assays, target cancer cells expressing a GFP-luciferase fusion protein and BMDMs or human peripheral blood monocyte–derived macrophages were cocultured in a 96-well cell culture plate. Cancer cells were cocultured with macrophages for phagocytosis, and the samples of cancer cells alone (without macrophages) were used as controls. For NHL Raji cells, rituximab was used. For colorectal cancer DLD1 and SW480 cells, cetuximab was used. For breast cancer SKBR3 cells, trastuzumab was used. Surviving cancer cells were quantified by reading the luminescence signals with a luminometer (Cytation 3 imaging reader, BioTek). The long-term phagocytosis rate was determined by normalizing the luminescence of surviving cancer cells in the sample group (coculture with macrophages) to that of the control group (cancer cells only). The phagocytosis index was normalized to the maximal response in every experiment. A long-term phagocytosis assay was used to test whether paclitaxel acted on cancer cells or macrophages for promoting the efficacy of antibodies (experiments in Fig. 3, A and B). Specifically, either BMDMs or DLD1 cells were pretreated with paclitaxel for 24 hours. After thoroughly washing with PBS three times, the cells were seeded in 96-well plates and subjected to phagocytosis assays with nontreated DLD1 cells or BMDMs in the presence of cetuximab. After 24 hours of coculturing, the surviving DLD1 cells were quantified by the luminescence signals.

For microscopy-based phagocytosis assays, BMDMs or human peripheral blood monocyte–derived macrophages treated with control vehicle or paclitaxel were stained with CellTrace-Green for 20 min. Target cancer cells were stained with pHrodo Red at a final concentration of 120 ng/ml for 30 min. After two times of PBS washes, target cancer cells were cocultured with macrophages for 2 hours with or without antibodies.

High-throughput screening assay

The FDA-approved oncology drug set including 147 currently approved anticancer small molecules was obtained from the Division of Cancer Treatment and Diagnosis at the National Cancer Institute (NCI). For the high-throughput screen, individual anticancer small-molecule compounds (10 μM) were incubated with 0.03×10^6 DLD1 cells expressing GFP-luciferase and 0.06×10^6 macrophages in the presence or absence of cetuximab in 96-well plates for 24 hours. Thereafter, luciferin was added into the plates and the luminescence signal was measured with Cytation 3. Wells containing DLD1 cells only in the presence of drugs were used as a control for calculating phagocytosis rate (phagocytosis rate = 0%). The normalized phagocytosis index was calculated as the ratio of phagocytosis rates of drug treatment to that of dimethyl sulfoxide (DMSO) control.

NF-κB reporter assay

A luminescence-based NF-κB reporter was generated on the basis of a GFP-based NF-κB reporter [a gift from S. Carpenter at the University of California, Santa Cruz (*77*)], as described in our previous study (*59*). Briefly, a RAW264.7 NF-κB reporter cell line was generated by infecting RAW264.7 cells with lentiviruses containing the luminescence-based NF-κB reporter in the presence of polybrene (8 μg/ml) for 48 hours.

Following overnight incubation, RAW264.7 NF-κB reporter lines were stimulated with lipopolysaccharide (LPS) (1 ng/ml) or paclitaxel (5, 2.5, 1.25, and 0.625 μM) for 8 hours. Unstimulated cells were used as a negative control. Luciferin was added to the cells, and luminescence signals were measured using a luminometer (Cytation3 imaging reader, BioTek). NF-κB activation was normalized to the negative control.

Mouse models

For the subcutaneous human NHL model, Raji cells expressing an enhanced GFP (eGFP)–luciferase protein were resuspended in RPMI with 25% Corning Matrigel Matrix (v/v) and injected into the back of $RAG2^{-/-}\gamma c^{-/-}$ mice. After the tumors were established, the mice were regrouped on the basis of the luminescence signals and treated with control vehicle, rituximab, paclitaxel, or a combination of rituximab and paclitaxel as indicated in the figure legend. For the systemic human NHL model, Raji cells expressing an eGFP-luciferase protein were slowly injected into $RAG2^{-/-}\gamma c^{-/-}$ mice through the tail vein (3×10^6 cells per mouse). Clinical-grade nab-paclitaxel obtained from City of Hope Helford Research Hospital was used for the in vivo study, which is better tolerated than solvent (Cremophor EL)–based paclitaxel (*39*, *40*). After 10 days, the animals were treated with vehicle (control) and/or rituximab as described in the figures and figure legends. Bioluminescence imaging was performed to monitor the tumor progression. Animal weights were recorded regularly, and end points of the mice were determined according to the Institutional Animal Care and Use Committee protocol approved by the Administrative Panel on Laboratory Animal Care at City of Hope Comprehensive Cancer Center.

For the mouse peritoneal colorectal cancer model, 2×10^5 SW480 cells expressing an eGFP-luciferase protein were injected into the peritoneal cavity of NSG mice. Five days later, the mice were regrouped on the basis of the bioluminescence signals and treated with control vehicle, cetuximab, nab-paclitaxel, or a combination of cetuximab and nab-paclitaxel intravenously. Tumor progression was monitored by bioluminescence imaging.

The colorectal PDX model was obtained from the Small Animal Studies Core at City of Hope Comprehensive Cancer Center [the patient had left-sided colorectal cancer, KRAS G12V and PIK3CA (G1049R) mutated, Microsatellite Stable]. After reviving on $RAG2^{-/-}\gamma c^{-/-}$ mice through subcutaneous transplantation, the cells were stained to be positive for human EGFR expression and transplanted to $RAG2^{-/-}\gamma c^{-/-}$ mice with 2 mm by 2 mm pieces. Two weeks after the transplantation, the mice were treated with control vehicle, cetuximab, nab-paclitaxel, or a combination of cetuximab and nab-paclitaxel intravenously. Tumor size and animal weight were measured regularly.

For evaluating phagocytosis of cancer cells by TAMs, SW480 cells expressing an eGFP-luciferase protein were injected into $RAG2^{-/-}\gamma c^{-/-}$ mice subcutaneously. Fourteen days after engraftment, the mice were treated with control vehicle, cetuximab, nab-paclitaxel, or a combination of cetuximab and nab-paclitaxel intravenously. The tumors were collected, digested to single-cell suspension, and

subjected to FACS analysis. TAMs were gated as $CD45^+F4/80^+$Sytox $blue^-$. Phagocytosis was quantified as the percentage of macrophages that phagocytosed cancer cells.

In vivo macrophage depletion

Clodronate liposomes and control liposomes (PBS) were purchased from Liposoma (The Netherlands). Macrophages were depleted in mice with the following treatment schedule: 200 μl of either clodronate or liposomal control was injected intravenously via the retro-orbital sinus 24 hours before treatment of the mice with intraperitoneal injection with SW480 (2×10^5) and/or cetuximab antibody. Three days after tumor injection, 100 μl of either clodronate or liposomal control was injected (intraperitoneally) to maintain the depletion of macrophages. Bioluminescence images were captured with Lago X (Spectral Instruments Imaging), and signals were analyzed with the Aura Image software. Mice were then sacrificed on day 7, and peritoneal fluid was collected for macrophage analysis by flow cytometry.

Flow cytometry analysis

Anti-mouse F4/80 (clone BM8, BioLegend), anti-mouse/human CD11b (clone M1/70, BioLegend), anti-mouse MHCII (clone M5/114.15.2, BioLegend), anti-mouse iNOS (clone W16030C, BioLegend), anti-mouse CD206 (clone C068C2, BioLegend), and anti-mouse CSF1R (clone AFS98, BioLegend) were used for FACS analyses. The antibodies were PE-, PE-Cy7–, allophycocyanin (APC)–, APC Cy7–, or Alexa Fluor 700–conjugated, or fluorophore-conjugated secondary antibodies were used. Sytox blue or Zombie Violet was used to exclude dead cells. Flow cytometry was performed using the BD LSRFortessa cell analyzers.

TAM analysis

$RAG2^{-/-}\gamma c^{-/-}$ mice were engrafted with the PDX colorectal tumor and treated with vehicle or nab-paclitaxel. A single-cell suspension was obtained after digesting the minced tumor tissue with Liberase TM enzymes (Thermo Fisher Scientific) and deoxyribonuclease I (Thermo Fisher Scientific) at 37°C for 1 hour. After the red blood cells were lysed with ACK lysis buffer, the single cells were filtered through a 70-μm cell strainer, treated with FcR blockers (Miltenyi) before being stained with the indicated antibodies, and subjected to flow cytometry analysis. TAMs were gated as $CD45^+F4/80^+$Zombie $Violet^-$. The expression of MHCII, iNOS, and CD206 was examined by flow cytometry analysis. For phospho-IκBα staining, the tumor cells were fixed with 4% paraformaldehyde (PFA) for 15 min. Thereafter, the cells were permeabilized with a permeabilization buffer (BioLegend) according to the manufacturer's instructions. The cells were then stained with anti–phospho-IκBα antibody and analyzed with flow cytometry.

BMDM polarization

BMDMs (1.6×10^6) were seeded in each well of a six-well petri dish plate and stimulated for 48 hours to induce M0 macrophages (IMDM with 10% FBS), M1-like macrophages [LPS (50 ng/ml) and IFNγ (10 ng/ml)], M2a-like macrophages [IL-4 (10 ng/ml)], and M2c-like macrophages [IL-10 (50 ng/ml) and TGFβ (transforming growth factor–β) (5 ng/ml)].

Cell fractionation

BMDMs (5×10^6) were seeded on a 10-cm petri dish plate for 24 hours and then treated with paclitaxel (5 μM) for 0, 30, 60, or 120 min. Subsequently, BMDMs were collected by trypsinization and washed with cold PBS. Cytoplasmic and nuclear protein fractions were isolated using nuclear and cytoplasmic extraction reagents (Abcam). Equal amounts of proteins were immunoblotted for NF-κB p65. The membranes with nuclear and cytoplasmic cell extracts were also probed for histone 3 or β-tubulin, respectively, to verify the purity of the fractions.

NF-κB nuclear translocation

BMDMs were plated on sterile 18-mm glass coverslips for 24 hours to allow cell attachment and then treated with DMSO or paclitaxel (5 μM) for 60 min. The cells were fixed with 4% PFA solution for 15 min at room temperature. After washing with PBS, the cells were permeabilized and blocked with PBS containing 0.1% Triton X-100 and 2% bovine serum albumin for 60 min. The coverslips were then incubated with 1:100 anti–NF-κB p65 in a humidified chamber overnight at 4°C. The coverslips were washed with PBS (3×10 min) at room temperature and incubated with Alexa Fluor 488 goat anti-rabbit IgG for 60 min at room temperature. The coverslips were washed with PBS (3×10 min) and mounted with antifade mounting medium with 4′,6-diamidino-2-phenylindole (VectaShield). Images were collected using a Leica DMI 4000B microscope. All images were processed with ImageJ (National Institutes of Health, Bethesda).

Western blotting

Protein extracts either from cell fractionation or radioimmunoprecipitation assay buffer–lysed cells were quantified by bicinchoninic acid assay (BCA) protein assay. Protein samples were diluted in loading buffer [62.5 mM tris-HCl (pH 6.8), 10% glycerol, 2% SDS, 0.01% bromophenol blue, and 100 mM dithiothreitol] and subjected to SDS–polyacrylamide gel electrophoresis. For immunoblotting, anti-IκBα, phospho-IκBα, p65, phospho-p65 (Ser^{536}), histone 3 (Cell Signaling Technology), β-tubulin (Sigma-Aldrich), or CSF1 (BioLegend) primary antibodies and horseradish peroxidase–conjugated anti-rabbit IgG or anti-mouse IgG secondary antibodies were used.

Gene knockdown by siRNAs in primary macrophages

The siGENOME SMARTpool and DharmaFECT 4 (Dharmacon) were used to knock down genes from BMDMs on a 96-well plate based on the manufacturer's instruction. Briefly, nontargeting control siRNA or siRNA of target genes was mixed with the transfection reagent DharmaFECT 4. After incubation for 30 min at room temperature, BMDMs were added and the cells were then cultured for another 48 hours followed by evaluating the gene knockdown efficiency by flow cytometry or long-term phagocytosis assay as described in the figure legend.

CRISPR-Cas9–mediated gene editing

The CRISPR-Cas9 system was used to suppress gene expression in primary macrophages from the CRISPR-Cas9 knockin mice [$Gt(ROSA)26Sor^{em1.1(CAG-cas9*,-EGFP)Rsky}$] (*49*), which expressed Cas9 proteins. Specifically, control sgRNA (AGUCCGGUCGAAAUCUGUAU), sgRNA targeting mouse CSF1R (CGGAUAAUGAACCCUCGCCA), or sgRNA targeting mouse Sirpα (UUUGCUCGUAGUCCUGCUGA) (*78*) was cloned into the vector pLKO5.sgRNA.EFS.tRFP for sgRNA delivery without Cas9. The vector pLKO5.sgRNA.EFS.tRFP was a gift from B. Ebert (Addgene, plasmid #57823) (*79*). The viruses were concentrated as previously reported (*80*). Bone marrow cells

were collected on day 1 and cultured in the presence of murine MCSF (10 ng/ml). On day 2, the concentrated lentivirus delivering control gRNA or gRNA targeting mouse CSF1R or Sirpα was added into the bone marrow cells together with polybrene (8 μg/ml). On day 4, the culture medium was replaced with fresh IMDM with 10% FBS containing MCSF (10 ng/ml). Thereafter, the cells were cultured for another 3 days and then used for experiments.

RNA sequencing

After 7 days of differentiation, BMDMs were treated with DMSO (control) or 10 μM paclitaxel for 24 hours, and total RNA was then extracted with an RNA extraction kit (Qiagen) and used for library preparation. Samples generated from three individual mice were submitted to Novogene for RNA sequencing as triplicates, which were performed on the Illumina NovaSeq 6000 platform. The clean reads were aligned to the reference genome mm10 using STAR 2.5.3a for generating mapped reads. Subsequently, the number of mapped clean reads was counted and normalized into fragments per kilobase of transcript per million reads (FPKM). FPKM values of 16,978 genes obtained from RNA sequencing were used as the original raw data and analyzed by the GSA algorithm. The differentially expressed genes (fold change > 2 and $P < 0.05$) were presented as a volcano plot. In this dataset, 381 genes were up-regulated and 178 genes were down-regulated after paclitaxel treatment.

Cytokine array

BMDM cells (5×10^5) were evenly plated into each well of a 24-well plate and treated with DMSO or paclitaxel (5 μM). After 24 hours, the medium was collected followed by removing cell debris through centrifugation and freezing at −80°C immediately. The cytokines/chemokines were measured with the Millipore MILLIPLEX Mouse Cytokine/Chemokine Kit by Eve Technologies.

Statistical analysis and graphing software

All data were statistically analyzed and graphed using Microsoft Excel or GraphPad Prism V.6 or V.8. Kaplan-Meier method and log-rank test were used to evaluate the overall survival between groups. The significant differences between groups were calculated via unpaired *t* test, analysis of variance (ANOVA), or log-linear regression analysis. The quantitative data in the study were presented as means ± SD. *P* values of less than 0.05 were considered statistically significant differences.

SUPPLEMENTARY MATERIALS

Supplementary material for this article is available at https://science.org/doi/10.1126/sciadv.abl9171

View/request a protocol for this paper from *Bio-protocol*.

REFERENCES AND NOTES

1. G. J. Weiner, Rituximab: Mechanism of action. *Semin. Hematol.* **47**, 115–123 (2010).
2. T. M. Habermann, E. A. Weller, V. A. Morrison, R. D. Gascoyne, P. A. Cassileth, J. B. Cohn, S. R. Dakhil, B. Woda, R. I. Fisher, B. A. Peterson, S. J. Horning, Rituximab-CHOP versus CHOP alone or with maintenance rituximab in older patients with diffuse large B-cell lymphoma. *J. Clin. Oncol.* **24**, 3121–3127 (2006).
3. E. H. Romond, E. A. Perez, J. Bryant, V. J. Suman, C. E. Geyer Jr., N. E. Davidson, E. Tan-Chiu, S. Martino, S. Paik, P. A. Kaufman, S. M. Swain, T. M. Pisansky, L. Fehrenbacher, L. A. Kutteh, V. G. Vogel, D. W. Visscher, G. Yothers, R. B. Jenkins, A. M. Brown, S. R. Dakhil, E. P. Mamounas, W. L. Lingle, P. M. Klein, J. N. Ingle, N. Wolmark, Trastuzumab plus adjuvant chemotherapy for operable HER2-positive breast cancer. *N. Engl. J. Med.* **353**, 1673–1684 (2005).
4. D. Cunningham, Y. Humblet, S. Siena, D. Khayat, H. Bleiberg, A. Santoro, D. Bets, M. Mueser, A. Harstrick, C. Verslype, I. Chau, E. Van Cutsem, Cetuximab monotherapy and cetuximab plus irinotecan in irinotecan-refractory metastatic colorectal cancer. *N. Engl. J. Med.* **351**, 337–345 (2004).
5. J. A. Bonner, P. M. Harari, J. Giralt, N. Azarnia, D. M. Shin, R. B. Cohen, C. U. Jones, R. Sur, D. Raben, J. Jassem, R. Ove, M. S. Kies, J. Baselga, H. Youssoufian, N. Amellal, E. K. Rowinsky, K. K. Ang, Radiotherapy plus cetuximab for squamous-cell carcinoma of the head and neck. *N. Engl. J. Med.* **354**, 567–578 (2006).
6. H. J. Lenz, Anti-EGFR mechanism of action: Antitumor effect and underlying cause of adverse events. *Oncology* **20**, 5–13 (2006).
7. C. A. Hudis, Trastuzumab—Mechanism of action and use in clinical practice. *N. Engl. J. Med.* **357**, 39–51 (2007).
8. F. S. Hodi, S. J. O'Day, D. F. McDermott, R. W. Weber, J. A. Sosman, J. B. Haanen, R. Gonzalez, C. Robert, D. Schadendorf, J. C. Hassel, W. Akerley, A. J. van den Eertwegh, J. Lutzky, P. Lorigan, J. M. Vaubel, G. P. Linette, D. Hogg, C. H. Ottensmeier, C. Lebbe, C. Peschel, I. Quirt, J. I. Clark, J. D. Wolchok, J. S. Weber, J. Tian, M. J. Yellin, G. M. Nichol, A. Hoos, W. J. Urba, Improved survival with ipilimumab in patients with metastatic melanoma. *N. Engl. J. Med.* **363**, 711–723 (2010).
9. M. R. Gilbert, J. J. Dignam, T. S. Armstrong, J. S. Wefel, D. T. Blumenthal, M. A. Vogelbaum, H. Colman, A. Chakravarti, S. Pugh, M. Won, R. Jeraj, P. D. Brown, K. A. Jaeckle, D. Schiff, V. W. Stieber, D. G. Brachman, M. Werner-Wasik, I. W. Tremont-Lukats, E. P. Sulman, K. D. Aldape, W. J. Curran Jr., M. P. Mehta, A randomized trial of bevacizumab for newly diagnosed glioblastoma. *N. Engl. J. Med.* **370**, 699–708 (2014).
10. E. B. Garon, N. A. Rizvi, R. Hui, N. Leighl, A. S. Balmanoukian, J. P. Eder, A. Patnaik, C. Aggarwal, M. Gubens, L. Horn, E. Carcereny, M. J. Ahn, E. Felip, J. S. Lee, M. D. Hellmann, O. Hamid, J. W. Goldman, J. C. Soria, M. Dolled-Filhart, R. Z. Rutledge, J. Zhang, J. K. Lunceford, R. Rangwala, G. M. Lubiniecki, C. Roach, K. Emancipator, L. Gandhi, K. Investigators, Pembrolizumab for the treatment of non-small-cell lung cancer. *N. Engl. J. Med.* **372**, 2018–2028 (2015).
11. S. C. Wei, C. R. Duffy, J. P. Allison, Fundamental mechanisms of immune checkpoint blockade therapy. *Cancer Discov.* **8**, 1069–1086 (2018).
12. S. L. Topalian, C. G. Drake, D. M. Pardoll, Immune checkpoint blockade: A common denominator approach to cancer therapy. *Cancer Cell* **27**, 450–461 (2015).
13. A. M. Scott, J. D. Wolchok, L. J. Old, Antibody therapy of cancer. *Nat. Rev. Cancer* **12**, 278–287 (2012).
14. L. Cassetta, J. W. Pollard, Targeting macrophages: Therapeutic approaches in cancer. *Nat. Rev. Drug Discov.* **17**, 887–904 (2018).
15. R. A. Franklin, W. Liao, A. Sarkar, M. V. Kim, M. R. Bivona, K. Liu, E. G. Pamer, M. O. Li, The cellular and molecular origin of tumor-associated macrophages. *Science* **344**, 921–925 (2014).
16. R. Noy, J. W. Pollard, Tumor-associated macrophages: From mechanisms to therapy. *Immunity* **41**, 49–61 (2014).
17. R. Stewart, S. A. Hammond, M. Oberst, R. W. Wilkinson, The role of Fc gamma receptors in the activity of immunomodulatory antibodies for cancer. *J. Immunother. Cancer* **2**, 29 (2014).
18. L. C. Carrascosa, A. A. van Beek, V. de Ruiter, M. Doukas, J. Wei, T. S. Fisher, K. Ching, W. Yang, K. van Loon, P. P. Boor, Y. S. Rakké, L. Noordam, P. Doornebosch, D. Grünhagen, K. Verhoef, W. G. Polak, J. N. M. IJzermans, I. Ni, Y. A. Yeung, S. Salek-Ardakani, D. Sprengers, J. Kwekkeboom, FcγRIIB engagement drives agonistic activity of Fc-engineered αOX40 antibody to stimulate human tumor-infiltrating T cells. *J. Immunother. Cancer* **8**, e000816 (2020).
19. R. A. Clynes, T. L. Towers, L. G. Presta, J. V. Ravetch, Inhibitory Fc receptors modulate in vivo cytotoxicity against tumor targets. *Nat. Med.* **6**, 443–446 (2000).
20. M. B. Overdijk, S. Verploegen, M. Bogels, M. van Egmond, J. J. Lammerts van Bueren, T. Mutis, R. W. J. Groen, E. Breij, A. C. M. Martens, W. K. Bleeker, P. W. H. I. Parren, Antibody-mediated phagocytosis contributes to the anti-tumor activity of the therapeutic antibody daratumumab in lymphoma and multiple myeloma. *MAbs* **7**, 311–321 (2015).
21. K. R. VanDerMeid, M. R. Elliott, A. M. Baran, P. M. Barr, C. C. Chu, C. S. Zent, Cellular cytotoxicity of next-generation CD20 monoclonal antibodies. *Cancer Immunol. Res.* **6**, 1150–1160 (2018).
22. M. Taskinen, M.-L. Karjalainen-Lindsberg, H. Nyman, L.-M. Eerola, S. Leppä, A high tumor-associated macrophage content predicts favorable outcome in follicular lymphoma patients treated with rituximab and cyclophosphamide-doxorubicin-vincristine-prednisone. *Clin. Cancer Res.* **13**, 5784–5789 (2007).
23. M. Pfreundschuh, E. Kuhnt, L. Trümper, A. Österborg, M. Trneny, L. Shepherd, D. S. Gill, J. Walewski, R. Pettengell, U. Jaeger, P.-L. Zinzani, O. Shpilberg, S. Kvaloy, P. de Nully Brown, R. Stahel, N. Milpied, A. López-Guillermo, V. Poeschel, S. Grass, M. Loeffler, N. Murawski; MabThera International Trial (MInT) Group, CHOP-like chemotherapy with or without rituximab in young patients with good-prognosis diffuse large-B-cell lymphoma: 6-year results of an open-label randomised study of the MabThera International Trial (MInT) Group. *Lancet Oncol.* **12**, 1013–1022 (2011).
24. W. Rastetter, A. Molina, C. A. White, Rituximab: Expanding role in therapy for lymphomas and autoimmune diseases. *Annu. Rev. Med.* **55**, 477–503 (2004).

25. R. S. Riley, C. H. June, R. Langer, M. J. Mitchell, Delivery technologies for cancer immunotherapy. *Nat. Rev. Drug Discov.* **18**, 175–196 (2019).
26. L. Milling, Y. Zhang, D. J. Irvine, Delivering safer immunotherapies for cancer. *Adv. Drug Deliv. Rev.* **114**, 79–101 (2017).
27. J. R. Ingram, O. S. Blomberg, J. T. Sockolosky, L. Ali, F. I. Schmidt, N. Pishesha, C. Espinosa, S. K. Dougan, K. C. Garcia, H. L. Ploegh, M. Dougan, Localized CD47 blockade enhances immunotherapy for murine melanoma. *Proc. Natl. Acad. Sci. U.S.A.* **114**, 10184–10189 (2017).
28. M. A. Aznar, N. Tinari, A. J. Rullan, A. R. Sanchez-Paulete, M. E. Rodriguez-Ruiz, I. Melero, Intratumoral delivery of immunotherapy-act locally, think globally. *J. Immunol.* **198**, 31–39 (2017).
29. C. Lossos, Y. Liu, K. E. Kolb, A. L. Christie, A. Van Scoyk, S. M. Prakadan, K. Shigemori, K. E. Stevenson, S. Morrow, O. D. Plana, C. Fraser, K. L. Jones, H. Liu, C. P. Pallasch, R. Modiste, Q.-D. Nguyen, J. W. Craig, E. A. Morgan, F. Vega, J. C. Aster, K. A. Sarosiek, A. K. Shalek, M. T. Hemann, D. M. Weinstock, Mechanisms of lymphoma clearance induced by high-dose alkylating agents. *Cancer Discov.* **9**, 944–961 (2019).
30. M. Liu, R. S. O'Connor, S. Trefely, K. Graham, N. W. Snyder, G. L. Beatty, Metabolic rewiring of macrophages by CpG potentiates clearance of cancer cells and overcomes tumor-expressed CD47–mediated 'don't-eat-me' signal. *Nat. Immunol.* **20**, 265–275 (2019).
31. Y. Shi, X. Fan, H. Deng, R. J. Brezski, M. Rycyzyn, R. E. Jordan, W. R. Strohl, Q. Zou, N. Zhang, Z. An, Trastuzumab triggers phagocytic killing of high HER2 cancer cells in vitro and in vivo by interaction with Fcγ receptors on macrophages. *J. Immunol.* **194**, 4379–4386 (2015).
32. J. Uchida, Y. Hamaguchi, J. A. Oliver, J. V. Ravetch, J. C. Poe, K. M. Haas, T. F. Tedder, The innate mononuclear phagocyte network depletes B lymphocytes through Fc receptor-dependent mechanisms during anti-CD20 antibody immunotherapy. *J. Exp. Med.* **199**, 1659–1669 (2004).
33. S. Rafiq, J. P. Butchar, C. Cheney, X. Mo, R. Trotta, M. Caligiuri, D. Jarjoura, S. Tridandapani, N. Muthusamy, J. C. Byrd, Comparative assessment of clinically utilized CD20-directed antibodies in chronic lymphocytic leukemia cells reveals divergent NK cell, monocyte, and macrophage properties. *J. Immunol.* **190**, 2702–2711 (2013).
34. N. Gul, L. Babes, K. Siegmund, R. Korthouwer, M. Bogels, R. Braster, G. Vidarsson, T. L. ten Hagen, P. Kubes, M. van Egmond, Macrophages eliminate circulating tumor cells after monoclonal antibody therapy. *J. Clin. Invest.* **124**, 812–823 (2014).
35. A. Roghanian, I. Teige, L. Martensson, K. L. Cox, M. Kovacek, A. Ljungars, J. Mattson, A. Sundberg, A. T. Vaughan, V. Shah, N. R. Smyth, B. Sheth, H. T. Chan, Z. C. Li, E. L. Williams, G. Manfredi, R. J. Oldham, C. I. Mockridge, S. A. James, L. N. Dahal, K. Hussain, B. Nilsson, J. S. Verbeek, G. Juliusson, M. Hansson, M. Jerkeman, P. W. Johnson, A. Davies, S. A. Beers, M. J. Glennie, B. Frendeus, M. S. Cragg, Antagonistic human FcγRIIB (CD32B) antibodies have anti-tumor activity and overcome resistance to antibody therapy in vivo. *Cancer Cell* **27**, 473–488 (2015).
36. F. H. Shand, S. Ueha, M. Otsuji, S. S. Koid, S. Shichino, T. Tsukui, M. Kosugi-Kanaya, J. Abe, M. Tomura, J. Ziogas, K. Matsushima, Tracking of intertissue migration reveals the origins of tumor-infiltrating monocytes. *Proc. Natl. Acad. Sci. U.S.A.* **111**, 7771–7776 (2014).
37. A. Lievre, J.-B. Bachet, D. Le Corre, V. Boige, B. Landi, J.-F. Emile, J.-F. Côté, G. Tomasic, C. Penna, M. Ducreux, P. Rougier, F. Penault-Llorca, P. Laurent-Puig, KRAS mutation status is predictive of response to cetuximab therapy in colorectal cancer. *Cancer Res.* **66**, 3992–3995 (2006).
38. S. Jaiswal, M. P. Chao, R. Majeti, I. L. Weissman, Macrophages as mediators of tumor immunosurveillance. *Trends Immunol.* **31**, 212–219 (2010).
39. E. Miele, G. P. Spinelli, E. Miele, F. Tomao, S. Tomao, Albumin-bound formulation of paclitaxel (Abraxane® ABI-007) in the treatment of breast cancer. *Int. J. Nanomedicine* **4**, 99–105 (2009).
40. W. J. Gradishar, Albumin-bound paclitaxel: A next-generation taxane. *Expert Opin. Pharmacother.* **7**, 1041–1053 (2006).
41. Y. Zhu, S. Yao, L. Chen, Cell surface signaling molecules in the control of immune responses: A tide model. *Immunity* **34**, 466–478 (2011).
42. S. Yao, Y. Zhu, L. Chen, Advances in targeting cell surface signalling molecules for immune modulation. *Nat. Rev. Drug Discov.* **12**, 130–146 (2013).
43. M. Feng, W. Jiang, B. Y. Kim, C. C. Zhang, Y.-X. Fu, I. L. Weissman, Phagocytosis checkpoints as new targets for cancer immunotherapy. *Nat. Rev. Cancer* **19**, 568–586 (2019).
44. S. R. Gordon, R. L. Maute, B. W. Dulken, G. Hutter, B. M. George, M. N. McCracken, R. Gupta, J. M. Tsai, R. Sinha, D. Corey, A. M. Ring, A. J. Connolly, I. L. Weissman, PD-1 expression by tumour-associated macrophages inhibits phagocytosis and tumour immunity. *Nature* **545**, 495–499 (2017).
45. M. A. Cannarile, M. Weisser, W. Jacob, A.-M. Jegg, C. H. Ries, D. Rüttinger, Colony-stimulating factor 1 receptor (CSF1R) inhibitors in cancer therapy. *J. Immunother. Cancer* **5**, 53 (2017).
46. E. R. Stanley, V. Chitu, CSF-1 receptor signaling in myeloid cells. *Cold Spring Harb. Perspect. Biol.* **6**, a021857 (2014).
47. Y.-j. Song, Y. Xu, X. Zhu, J. Fu, C. Deng, H. Chen, H. Xu, G. Song, J. Lu, Q. Tang, Immune landscape of the tumor microenvironment identifies prognostic gene signature CD4/CD68/CSF1R in osteosarcoma. *Front. Oncol.* **10**, 1198 (2020).
48. D. G. DeNardo, D. J. Brennan, E. Rexhepaj, B. Ruffell, S. L. Shiao, S. F. Madden, W. M. Gallagher, N. Wadhwani, S. D. Keil, S. A. Junaid, H. S. Rugo, E. S. Hwang, K. Jirstrom, B. L. West, L. M. Coussens, Leukocyte complexity predicts breast cancer survival and functionally regulates response to chemotherapy. *Cancer Discov.* **1**, 54–67 (2011).
49. V. T. Chu, T. Weber, R. Graf, T. Sommermann, K. Petsch, U. Sack, P. Volchkov, K. Rajewsky, R. Kuhn, Efficient generation of Rosa26 knock-in mice using CRISPR/Cas9 in C57BL/6 zygotes. *BMC Biotechnol.* **16**, 4 (2016).
50. S. M. Pyonteck, L. Akkari, A. J. Schuhmacher, R. L. Bowman, L. Sevenich, D. F. Quail, O. C. Olson, M. L. Quick, J. T. Huse, V. Teijeiro, M. Setty, C. S. Leslie, Y. Oei, A. Pedraza, J. Zhang, C. W. Brennan, J. C. Sutton, E. C. Holland, D. Daniel, J. A. Joyce, CSF-1R inhibition alters macrophage polarization and blocks glioma progression. *Nat. Med.* **19**, 1264–1272 (2013).
51. H. Ohno, K. Kubo, H. Murooka, Y. Kobayashi, T. Nishitoba, M. Shibuya, T. Yoneda, T. Isoe, A c-fms tyrosine kinase inhibitor, Ki20227, suppresses osteoclast differentiation and osteolytic bone destruction in a bone metastasis model. *Mol. Cancer Ther.* **5**, 2634–2643 (2006).
52. R. Advani, I. Flinn, L. Popplewell, A. Forero, N. L. Bartlett, N. Ghosh, J. Kline, M. Roschewski, A. LaCasce, G. P. Collins, T. Tran, J. Lynn, J. Y. Chen, J.-P. Volkmer, B. Agoram, J. Huang, R. Majeti, I. L. Weissman, C. H. Takimoto, M. P. Chao, S. M. Smith, CD47 blockade by Hu5F9-G4 and rituximab in non-Hodgkin's lymphoma. *N. Engl. J. Med.* **379**, 1711–1721 (2018).
53. F. Di Fiore, F. Blanchard, F. Charbonnier, F. Le Pessot, A. Lamy, M. Galais, L. Bastit, A. Killian, R. Sesboüé, J. Tuech, A. M. Queuniet, B. Paillot, J. C. Sabourin, F. Michot, P. Michel, T. Frebourg, Clinical relevance of KRAS mutation detection in metastatic colorectal cancer treated by cetuximab plus chemotherapy. *Br. J. Cancer* **96**, 1166–1169 (2007).
54. R. Pirker, J. R. Pereira, J. Von Pawel, M. Krzakowski, R. Ramlau, K. Park, F. De Marinis, W. E. Eberhardt, L. Paz-Ares, S. Störkel, K.-M. Schumacher, A. von Heydebreck, I. Celik, K. J. O'Byrne, EGFR expression as a predictor of survival for first-line chemotherapy plus cetuximab in patients with advanced non-small-cell lung cancer: Analysis of data from the phase 3 FLEX study. *Lancet Oncol.* **13**, 33–42 (2012).
55. F. Cappuzzo, G. Finocchiaro, E. Rossi, P. Jänne, C. Carnaghi, C. Calandri, K. Bencardino, C. Ligorio, F. Ciardiello, T. Pressiani, A. Destro, M. Roncalli, L. Crino, W. A. Franklin, A. Santoro, M. Varella-Garcia, EGFR FISH assay predicts for response to cetuximab in chemotherapy refractory colorectal cancer patients. *Ann. Oncol.* **19**, 717–723 (2008).
56. M. Lecoultre, V. Dutoit, P. R. Walker, Phagocytic function of tumor-associated macrophages as a key determinant of tumor progression control: A review. *J. Immunother. Cancer* **8**, e001408 (2020).
57. D. V. Tassev, N. K. Cheung, Monoclonal antibody therapies for solid tumors. *Expert Opin. Biol. Ther.* **9**, 341–353 (2009).
58. M. T. Spiotto, P. Yu, D. A. Rowley, M. I. Nishimura, S. C. Meredith, T. F. Gajewski, Y.-X. Fu, H. Schreiber, Increasing tumor antigen expression overcomes "ignorance" to solid tumors via crosspresentation by bone marrow-derived stromal cells. *Immunity* **17**, 737–747 (2002).
59. X. Cao, B. Li, J. Chen, J. Dang, S. Chen, E. G. Gunes, B. Xu, L. Tian, S. Muend, M. Raoof, C. Querfeld, J. Yu, S. T. Rosen, Y. Wang, M. Feng, Effect of cabazitaxel on macrophages improves CD47-targeted immunotherapy for triple-negative breast cancer. *J. Immunother. Cancer* **9**, e002022 (2021).
60. C. J. Fitzer-Attas, M. Lowry, M. T. Crowley, A. J. Finn, F. Meng, A. L. DeFranco, C. A. Lowell, Fcγ receptor–mediated phagocytosis in macrophages lacking the Src family tyrosine kinases Hck, Fgr, and Lyn. *J. Exp. Med.* **191**, 669–682 (2000).
61. M. Feng, J. Y. Chen, R. Weissman-Tsukamoto, J.-P. Volkmer, P. Y. Ho, K. M. McKenna, S. Cheshier, M. Zhang, N. Guo, P. Gip, S. S. Mitra, I. L. Weissman, Macrophages eat cancer cells using their own calreticulin as a guide: Roles of TLR and Btk. *Proc. Natl. Acad. Sci. U.S.A.* **112**, 2145–2150 (2015).
62. P. Sharma, J. P. Allison, Immune checkpoint targeting in cancer therapy: Toward combination strategies with curative potential. *Cell* **161**, 205–214 (2015).
63. P. Schmid, S. Adams, H. S. Rugo, A. Schneeweiss, C. H. Barrios, H. Iwata, V. Dieras, R. Hegg, S. A. Im, G. Shaw Wright, V. Henschel, L. Molinero, S. Y. Chui, R. Funke, A. Husain, E. P. Winer, S. Loi, L. A. Emens; IMpassion130 Trial Investigators, Atezolizumab and nab-paclitaxel in advanced triple-negative breast cancer. *N. Engl. J. Med.* **379**, 2108–2121 (2018).
64. C. W. Wanderley, D. F. Colon, J. P. M. Luiz, F. F. Oliveira, P. R. Viacava, C. A. Leite, J. A. Pereira, C. M. Silva, C. R. Silva, R. L. Silva, C. A. Speck-Hernandez, J. M. Mota, J. C. Alves-Filho, R. C. Lima-Junior, T. M. Cunha, F. Q. Cunha, Paclitaxel reduces tumor growth by reprogramming tumor-associated macrophages to an M1 profile in a TLR4-dependent manner. *Cancer Res.* **78**, 5891–5900 (2018).
65. X. Zhong, H. N. Lee, S. H. Kim, S. A. Park, W. Kim, Y. N. Cha, Y. J. Surh, Myc-nick promotes efferocytosis through M2 macrophage polarization during resolution of inflammation. *FASEB J.* **32**, 5312–5325 (2018).

66. B. Rayet, C. Gelinas, Aberrant rel/nfkb genes and activity in human cancer. *Oncogene* **18**, 6938–6947 (1999).
67. R. D. Leek, C. E. Lewis, R. Whitehouse, M. Greenall, J. Clarke, A. L. Harris, Association of macrophage infiltration with angiogenesis and prognosis in invasive breast carcinoma. *Cancer Res.* **56**, 4625–4629 (1996).
68. Q. Feng, W. Chang, Y. Mao, G. He, P. Zheng, W. Tang, Y. Wei, L. Ren, D. Zhu, M. Ji, Y. Tu, X. Qin, J. Xu, Tumor-associated macrophages as prognostic and predictive biomarkers for postoperative adjuvant chemotherapy in patients with stage II colon cancer. *Clin. Cancer Res.* **25**, 3896–3907 (2019).
69. H. L. Matlung, K. Szilagyi, N. A. Barclay, T. K. van den Berg, The CD47-SIRPα signaling axis as an innate immune checkpoint in cancer. *Immunol. Rev.* **276**, 145–164 (2017).
70. J. G. Egen, M. S. Kuhns, J. P. Allison, CTLA-4: New insights into its biological function and use in tumor immunotherapy. *Nat. Immunol.* **3**, 611–618 (2002).
71. F. J. Pixley, E. R. Stanley, CSF-1 regulation of the wandering macrophage: Complexity in action. *Trends Cell Biol.* **14**, 628–638 (2004).
72. A. Ramesh, S. Kumar, D. Nandi, A. Kulkarni, CSF1R-and SHP2-inhibitor-loaded nanoparticles enhance cytotoxic activity and phagocytosis in tumor-associated macrophages. *Adv. Mater.* **31**, 1904364 (2019).
73. F. Lei, N. Cui, C. Zhou, J. Chodosh, D. G. Vavvas, E. I. Paschalis, CSF1R inhibition by a small-molecule inhibitor is not microglia specific; affecting hematopoiesis and the function of macrophages. *Proc. Natl. Acad. Sci. U.S.A.* **117**, 23336–23338 (2020).
74. E. Richardsen, R. D. Uglehus, S. H. Johnsen, L.-T. Busund, Macrophage-colony stimulating factor (CSF1) predicts breast cancer progression and mortality. *Anticancer Res.* **35**, 865–874 (2015).
75. L. Wang, D. L. Simons, X. Lu, T. Y. Tu, C. Avalos, A. Y. Chang, F. M. Dirbas, J. H. Yim, J. Waisman, P. P. Lee, Breast cancer induces systemic immune changes on cytokine signaling in peripheral blood monocytes and lymphocytes. *EBioMedicine* **52**, 102631 (2020).
76. J. Chen, X. Cao, B. Li, Z. Zhao, S. Chen, S. W. T. Lai, S. A. Muend, G. K. Nossa, L. Wang, W. Guo, J. Ye, P. P. Lee, M. Feng, Warburg effect is a cancer immune evasion mechanism against macrophage immunosurveillance. *Front. Immunol.* **11**, 621757 (2021).
77. S. Covarrubias, E. K. Robinson, B. Shapleigh, A. Vollmers, S. Katzman, N. Hanley, N. Fong, M. T. McManus, S. Carpenter, CRISPR/Cas-based screening of long non-coding RNAs (lncRNAs) in macrophages with an NF-κB reporter. *J. Biol. Chem.* **292**, 20911–20920 (2017).
78. N. E. Sanjana, O. Shalem, F. Zhang, Improved vectors and genome-wide libraries for CRISPR screening. *Nat. Methods* **11**, 783–784 (2014).
79. D. Heckl, M. S. Kowalczyk, D. Yudovich, R. Belizaire, R. V. Puram, M. E. McConkey, A. Thielke, J. C. Aster, A. Regev, B. L. Ebert, Generation of mouse models of myeloid malignancy with combinatorial genetic lesions using CRISPR-Cas9 genome editing. *Nat. Biotechnol.* **32**, 941–946 (2014).
80. M. Nasri, A. Karimi, M. Allahbakhshian Farsani, Production, purification and titration of a lentivirus-based vector for gene delivery purposes. *Cytotechnology* **66**, 1031–1038 (2014).

Acknowledgments: We thank the excellent technical support of Core Facilities at City of Hope, including the Analytical Cytometry, Animal Resource Center, Small Animal Imaging, and Light Microscopy Core Facilities supported by the NCI of the NIH under award number P30CA033572. We thank S. Chen, S. Muend, S. Lai, Y. Guo, and J. Wu for helpful discussions, technical assistance, or proofreading. Figure 1C was created with BioRender.com.
Funding: This work was supported by the Lymphoma Research Foundation Postdoctoral Fellowship (to X.C.); NIH R01CA255250 (to M.F.), R01NS106170 (to J.Y.), R01AI129582 (to J.Y.), R01CA247550 (to J.Y.), and R01CA068458 (to J.Y.); Damon Runyon-Dale F. Frey Award for Breakthrough Scientists DFS-22-16 (to M.F.); the Margaret E. Early Medical Research Trust Grant (to M.F.); the V Foundation for Cancer Research V Scholar Award (V2018-012) (to M.F.); and the startup research funding from City of Hope (to M.F.). Funds from anonymous donors helped accelerate these studies. **Author contributions:** X.C. and M.F. conceived the study. X.C., J.C., B.L., J.D., W.Z., X.Z., and M.F. contributed to the investigation. X.C., J.C., J.D., and M.F. analyzed the data. C.W. and M.G.F. generated the PDX model and contributed to scientific input. M.R., Z.S., and J.Y. contributed to experimental design and scientific input. X.C. and M.F. prepared the figures and wrote and edited the manuscript. M.F. supervised the laboratory. **Competing interests:** M.F. is an inventor on a patent related to this work filed by Stanford University (U.S. Patent 10780117, filed on 21 January 2016, published on 22 September 2020). The remaining authors declare no competing interests. **Data and materials availability:** All data needed to evaluate the conclusions in the paper are present in the paper and/or the Supplementary Materials.

Submitted 13 August 2021
Accepted 26 January 2022
Published 18 March 2022
10.1126/sciadv.abl9171